UNIVERSITY OF CALIFORNIA

Los Angeles

Pick-up Ion Trajectories in a Comet Model

A thesis submitted in partial satisfaction of the requirements for the degree Master of Science in Geophysics and Space Physics

by

Charles David Kimmel

1986

UNCLASSIFIED
SECURITY CLASSIFICATION OF THIS PAGE (When Data Entered)

AD-A176 618

REPORT DOCUMENTATION PAGE

BEFORE COMPLETING FORM

1. REPORT NUMBER: AFIT/CI/NR 87-18T	2. GOVT ACCESSION NO.
3. RECIPIENT'S CATALOG NUMBER	
4. TITLE (and Subtitle): Pick-up Ion Trajectories in a Comet Model	5. TYPE OF REPORT & PERIOD COVERED: THESIS/DISSERTATION
	6. PERFORMING ORG. REPORT NUMBER
7. AUTHOR(s): Charles David Kimmel	8. CONTRACT OR GRANT NUMBER(s)
9. PERFORMING ORGANIZATION NAME AND ADDRESS: AFIT STUDENT AT: Univ of California	10. PROGRAM ELEMENT, PROJECT, TASK AREA & WORK UNIT NUMBERS
11. CONTROLLING OFFICE NAME AND ADDRESS: AFIT/NR, WPAFB OH 45433-6583	12. REPORT DATE: 1986
	13. NUMBER OF PAGES: 78
14. MONITORING AGENCY NAME & ADDRESS (if different from Controlling Office)	15. SECURITY CLASS. (of this report): UNCLASSIFIED
	15a. DECLASSIFICATION DOWNGRADING SCHEDULE

16. DISTRIBUTION STATEMENT (of this Report)

APPROVED FOR PUBLIC RELEASE; DISTRIBUTION UNLIMITED

17. DISTRIBUTION STATEMENT (of the abstract entered in Block 20, if different from Report)

18. SUPPLEMENTARY NOTES

APPROVED FOR PUBLIC RELEASE: IAW AFR 190-1

LYNN E. WOLAVER 20JAN87
Dean for Research and
Professional Development
AFIT/NR

19. KEY WORDS (Continue on reverse side if necessary and identify by block number)

20. ABSTRACT (Continue on reverse side if necessary and identify by block number)

ATTACHED

DD FORM 1 JAN 73 1473 EDITION OF 1 NOV 65 IS OBSOLETE

SECURITY CLASSIFICATION OF THIS PAGE (When Data Entered)

The thesis of Charles David Kimmel is approved.

Robert L. McPherron

George L. Siscoe

Janet G. Luhmann

Christopher T. Russell, Committee Chair

University of California, Los Angeles

1986

DEDICATION

To my wife, Mary Kay, and son, Christopher David,

for their never-ending support and encouragement.

Also to my mom and dad,

and to my brother, Tedd, and his wife, Julie,

who were with me each step of the way.

CONTENTS

LIST OF FIGURES

ACKNOWLEDGMENTS

I would like to thank the members of my thesis committee for their valuable suggestions and support. In particular, I would like to thank Janet Luhmann for her outstanding guidance and patience throughout the project.

I would also like to thank my fellow graduate students, Kurt Moore and John Phillips, for their computer expertise and camaraderie.

Finally, I'd like to thank Julie Knaack for her marvelous talent and skill in putting this project into final form.

ABSTRACT OF THE THESIS

Pick-up Ion Trajectories

in a Comet Model

by

Charles David Kimmel

Master of Science in Geophysics and Space Physics

University of California, Los Angeles, 1986

Professor Christopher T. Russell, Chair

In-situ measurements at Comets Giacobini-Zinner and Halley reveal the presence of energetic cometary ions accelerated to energies at times over 100 keV. This study investigates how the underlying large-scale magnetic field and velocity structure of an idealized comet, as represented by an MHD simulation, leads to the acceleration of these particles. Single particle trajectories have been computed using the results from Fedder and coworkers' MHD simulation of comets for the background magnetic and convection electric fields. For the present numerical model, it is assumed that the particles are not scattered by fluctuations in the field and plasma. In this scatter-free limit, the trajectories of initially cold cometary ions which accelerate due to the large-scale convection electric field are more widely dispersed in the plane of —>

the interplanetary magnetic field than in the orthogonal plane. Ions created closest to the nucleus focus into the tail current sheet, while those ions created in the outer coma diverge from the tail axis in response to gradient and curvature drifts. Those ions initially formed close to the nucleus have a lower energy, forming the cold plasma sheet, while the ions created in the outer coma have greater energy and populate the hot "wings" that extend far from the tail axis. The results suggest that the distinctive double-peaked time series seen in the observations of energetic pick-up ions arises from control of the particle trajectory by the large-scale plasma and field structure of the comet.

Chapter I

INTRODUCTION

Since recorded history began, comets have awakened the attention of their occasional witnesses due to their unexpected and sometimes spectacular appearance. To Aristotle, these graceful visitors in the sky were nothing more than vapors, exhaled from the earth, rising to the upper atmosphere. The early Greek astronomers named these fiery apparitions "aster komets," or "long-haired stars." From the earliest surviving reference to a comet, dating from the Fifteenth Century B.C. until the present age, comets have been linked with disaster. Today there is scientific debate over the premise that comets were responsible for the extinction of the dinosaurs. Even the word "apparition," which is used to describe the presence of a comet in our skies, has ominous and supernatural overtones.

In spite of our superstitious nature, much progress has been made in our understanding of the nature of comets. In 1577, Tycho Brahe determined that these "atmospheric phenomena" were actually far more distant than the moon. Edmund Halley made use for the first time of Newton's theory of gravitation to compute parabolic orbits of 24 comets observed up to 1698. In the present century, theories to explain the structure of comets are being compared to actual spacecraft observations.

The most generally accepted view of a comet today is the icy conglomerate or "dirty snowball" model first proposed in 1950 by F.L. Whipple (1950). In this model, a kilometer-sized nucleus is composed of dust and ice. Surrounding the nucleus and concealing it from observation is the cometary atmosphere which may extend up to several million kilometers in diameter. The visible part of his atmosphere is called the coma. At large heliocentric distances, most of the comet luminescence is due to sunlight scattered by the dust particles, but as the comet gets closer to the sun, visible and UV solar radiation dissociates and excites molecules which reradiate at the same or longer wavelengths. By the time comets are in the region of the terrestrial planets, most of their light comes from fluorescent radiation. One or more tails, directed away from the sun, extend behind the atmosphere. From observations of comet tails, Biermann (1951) was convinced that there was a stream of particles flowing continuously outward from the sun--the solar wind.

Two types of visible comet tails are known today: dust tails and plasma tails. Dust tails typically consist of solid, micrometer-size particles that have been pushed away from the coma by solar radiation pressure resulting from sunlight striking the dust grains. As the dust particles increase their distance from the sun, they slow down because of the conservation of angular momentum, which results in a curvature of the dust tail in the direction opposite to the comet's motion. Ion tails, in contrast to dust tails, are straight. The magnetic field associated with the solar wind drag the ions of the cometary coma in the antisolar direction and gives rise to the ion tail. Ion tails can reach lengths of 10^{8} km.

The interaction between the comet and the solar wind provides the framework for understanding how ions from the comet nucleus are accelerated or picked up by the solar wind--hence the term "pick-up ions." The ion pick-up process is illustrated in Figure 1. The following discussion assumes a comet-centered reference frame (i.e., one in which the nucleus is stationary at the origin). The solar wind, consisting of protons and electrons, and its magnetic field flow toward the comet at typical speeds of 400 km/s. Moving radially outward at 1 km/s, neutral molecules escape from the comet's surface. These molecules become ionized during their outbound journey, either by photoionization or charge exchange processes. Since these newly created cometary ions now have a net electric charge, they are immediately "accelerated" or "picked up" on the solar wind's magnetic field lines and are carried antisunward. Because the solar wind has had mass added to it in the form of these cometary ions, it must slow down to conserve momentum. This deceleration process continues as progressively more ions are captured during the solar wind's flight toward the inner atmosphere. Eventually a point is reached where so many ions have been captured and the flow has been so decelerated that the outward pressures from the ions and other gases closer to the nucleus are balanced by the inward pressures exerted by the solar wind carrying the captured ions. At this point, the flow of the solar wind stagnates. The magnetic field of the solar wind, which has been continuously compressed, forms a magnetic barrier at the stagnation point. Typically this stagnation point occurs a few thousands of kilometers from the nucleus--far inside the cometary atmosphere. Since the comet is an obstacle to the solar wind, a "bow

shock" is formed upstream of the comet. Far off to the sides of the comet, fewer ions are captured, and consequently, the solar wind is not as significantly impeded. The magnetic fields in these areas are connected to fields in the barrier and drape around the comet forming two lobes of opposite magnetic polarity (Figure 2) (Alfvén, 1957). The draped field lines, or magnetic tail of the comet, focus the fluorescing cometary ions to form the visible ion tail.

Until 1985, no *in situ* observations of comets existed with which to compare the various numerical simulations and theories of plasma physics. On September 11, 1985, the International Cometary Explorer (ICE) became the first spacecraft ever to intercept a comet, passing through the tail of Comet Giacobini-Zinner. This short-period comet was originally discovered by M. Giacobini at Nice, France, in 1900, and was rediscovered in 1913 by E. Zinner at Bamberg, Germany. Its elliptical orbit has a period of 6.5 years and lies between the orbits of Earth and Jupiter. At the time of the ICE encounter, the comet was six days past its closest approach to the sun (perihelion at 1.03 AU) and was crossing the ecliptic plane at an angle of 30 °. Giacobini-Zinner made a north to south pass across the spacecraft at a relative speed of 21 km/s. ICE passed 7800 km from the nucleus on the antisunward side.

The ICE observations of singly ionized water molecules (H_2O^+) at Comet Giacobini-Zinner provided first-hand information about a significant constituent of a comet. The interaction of these ions with the solar wind produces the distinctive ion coma and tail of the comet. Understanding the behavior of these ions and the process by which the ions are assimilated or "picked up" in the solar wind increases the knowledge of comets and space

ION PICK UP PROCESS

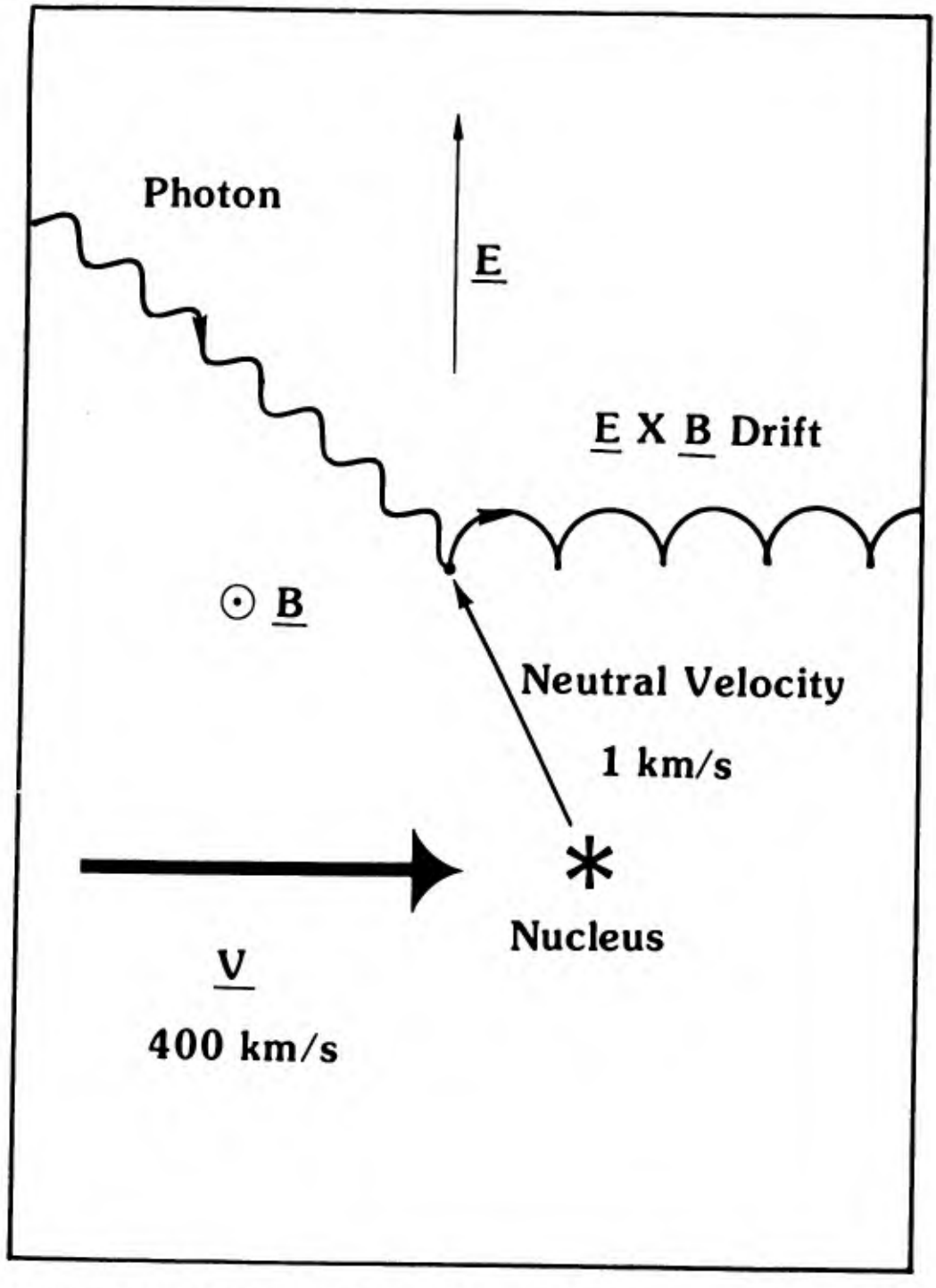

Figure 1. In the comet's reference frame, the solar wind velocity ($\underline{V}$) and magnetic field ($\underline{B}$) create a convection electric field ($\underline{E} = -\underline{V} \times \underline{B}$). A neutral molecule expands away from the comet nucleus at 1 km/s. After photoionization (or charge exchange), the ion responds to the magnetic and electric fields, drifting along a cycloidal path due to $\underline{E} \times \underline{B}$.

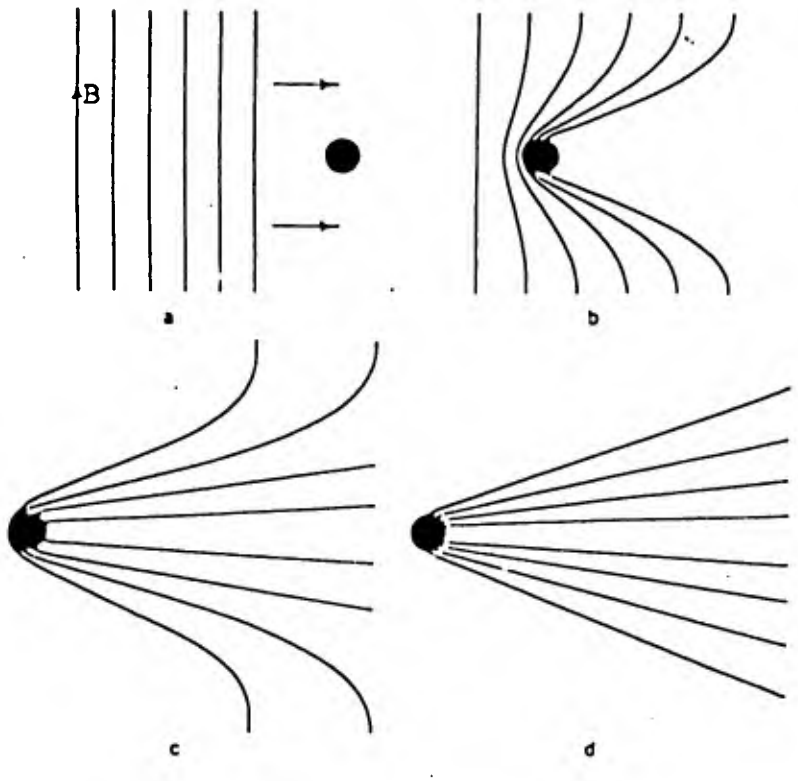

Figure 2. The imbedded magnetic field in the solar wind drapes around the comet nucleus due to mass loading effects, forming two lobes of oppositely directed field lines (Alfvén, 1957).

plasma physics. The properties of the picked-up ions at any one point in space depend not only on local conditions but also on the trajectory over which the particle has traveled. Thus, it is not trivial to determine the expected properties of these picked-up ions. This report describes a detailed study of the trajectories of these cometary pick-up ions. The results of a magnetohydrodynamic (MHD) simulation of the interaction of Comet Giacobini-Zinner with the solar wind (Fedder, 1986) are used to describe the electric and magnetic fields in which the particles move. A selected subset of the cometary particles comprising the MHD simulation is followed numerically in these fields. This subset of particles is chosen to model the radial density distribution of the cometary atmosphere. The properties of this particle "data" set are then analyzed and the results are compared with spacecraft observations. Effects of wavelike fluctuations are not specifically considered here. Rather, this study concentrates on the underlying order that must be imposed on the cometary ion distribution by the average plasma behavior in the coma.

Chapter II

ION-PICK-UP OBSERVATIONS

When the International Sun-Earth Explorer Three (ISEE-3) was launched in August 1978, there was no comet intercept planned. At that time, ISEE-3 was part of a joint NASA/ESA program designed to study the earth's magnetosphere. ISEE-3's mission was to make field and particle measurements of the solar wind 1.5 million km ($\sim 30 R_e$) sunward from the earth. A second phase in ISEE-3's mission began four years later, in 1982, when the spacecraft was moved to explore the distant magnetotail far beyond the moon's orbit. The third phase of ISEE-3 began in December 1983, when the spacecraft passed within 120 km of the moon and was propelled out of the earth-moon system to start a two-year journey to encounter Comet Giacobini-Zinner at a distance of 70 million km, or 0.47 AU, from earth. At this point, the spacecraft was renamed International Cometary Explorer (ICE).

The ICE mission to Comet Giacobini-Zinner provided the first *in situ* measurements of freshly ionized cometary particles and of their dynamics. The science payload of the ICE spacecraft carried an ultra-low-energy charge analyzer (ULECA) of the University of Maryland/Max-Planck Institut für Aeronomie (Hovestadt et al., 1978). The ULECA sensor was originally designed to measure H^+, He^{2+}, and highly ionized heavy ($\geq$12 atomic mass

units) particles found in the solar wind by simultaneously determining energy per charge and total energy for a particle. Although the instrument was not designed to measure singly ionized heavy ions such as those found in comets, given a sufficiently high flux rate, the instrument becomes sensitive to such ions. Due to an early failure of the solar wind analyzer, resolution in the energy range of 0-1 keV was lost. The instrument was only able to detect ions whose energies were greater than 30 keV. The ULECA sensor samples particles in the ecliptic plane in eight 45° sectors, with an acceptance angle of $\pm 30°$ out of the ecliptic plane.

The spacecraft observations proved to be exciting. For the first time, cometary ions were detected at distances of approximately 1×10^6 km from the nucleus. The counting rate profile of energetic ions detected by the ICE spacecraft is displayed in Figure 3. The top panel of the figure displays results for 35 keV ions using 34-minute averages. The insert represents an approximately scaled drawing of the Giacobini-Zinner cometary bow wave and tail regions. As illustrated in Figure 3, two peaks in the counting rate profile are evident. These peaks corresponded to a counting rate of approximately 7.5 counts per second during the inbound approach and nearly 10 counts per second during the outbound pass. The counting profile drops to near background levels (approximately 1 count per second) for 30 minutes centered on the tail axis. Prior to the inbound peak and after the outbound peak, normal background counts were detected. This "double-peaked" distribution in count rates was not restricted to only 35 keV ions. The Energetic Particle Anisotropy Spectrometer (EPAS) also observed large fluxes

of energetic ions (Hynds et al., 1986). The energy of these ions is higher, in the 65-95 keV range, but the results display the characteristic double-peaked signature, as illustrated in the bottom panel of Figure 3. Particles with energies of up to approximately 150 keV were also observed, but are not the subject of this study. The pick-up process can only accelerate water ions up to approximately 60 keV, given an upstream solar wind velocity of 400 km/s. To achieve the higher energy levels, some stochastic process must be involved (i.e., Fermi acceleration).

The two most frequently cited theoretical treatments of cometary ions have serious flaws and neither predict the double-peaked distribution observed by ICE. By concentrating on the local plasma kinetic aspects of ion pick-up (cf. Wu et al., 1986), the plasma instabilities associated with the production of the cold, heavy ion population in the flowing solar wind is examined, but the global picture is missing. Conversely, global fluid models of the solar wind plasma and magnetic field (Schmidt and Wegmann, 1982; Fedder and Lyon, 1986; Boice et al., 1986) while nicely illustrating large-scale effects due to ions, usually ignore the particle behavior and cometary ion assimilation process.

A third approach, used in this project, ties together the two previous methods of description and also explains the double-peaked spatial distribution of ions. By calculating trajectories of initially cold ions found in a global model of the comet's background plasma and field structure, unique information about the effect of the background structure on the picked-up ions is obtained. Such an approach neglects scattering of particle trajectories by turbulent

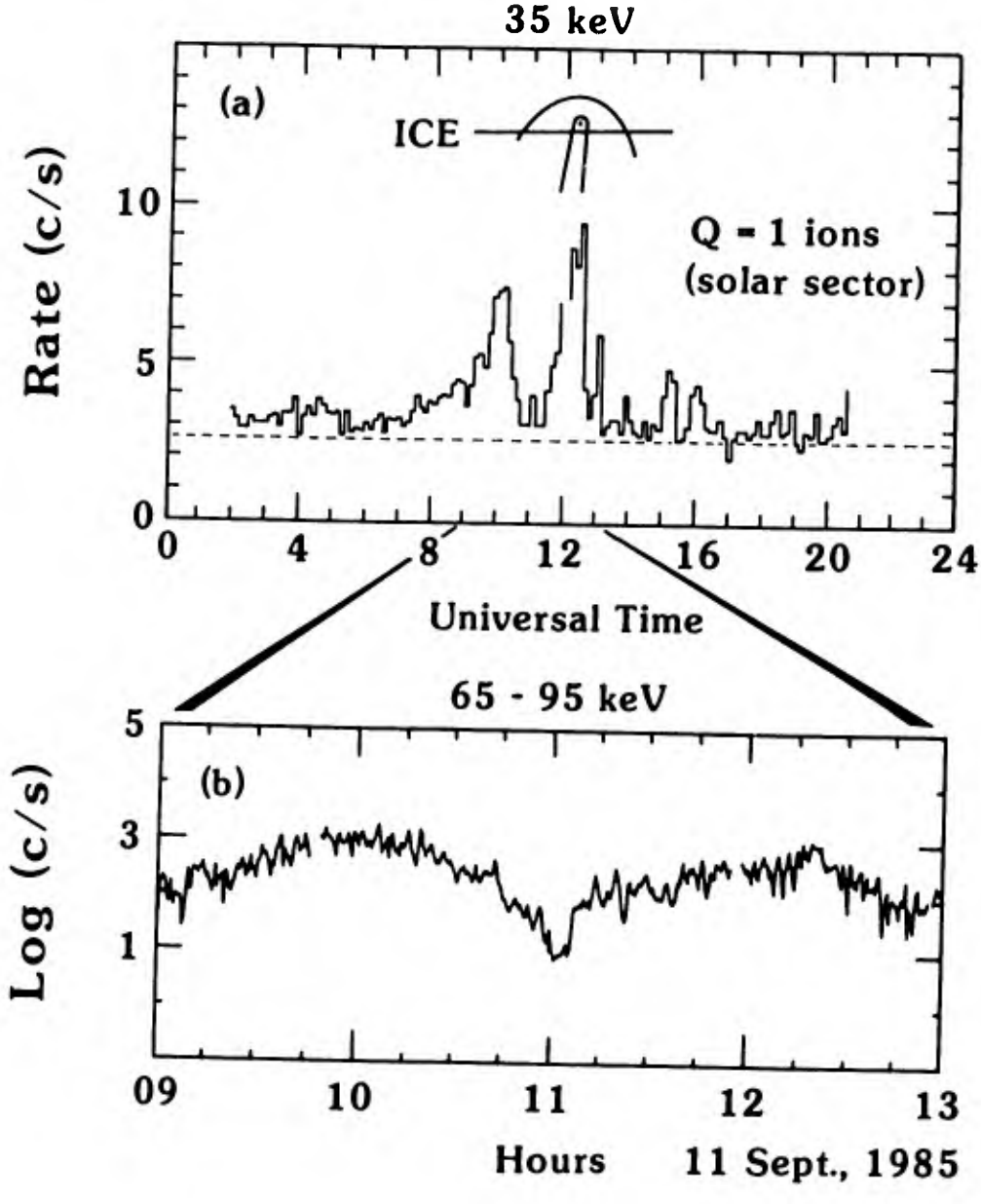

Figure 3. Data from ICE spacecraft for 35 keV ions (a) and 65-95 keV ions (b). The ICE trajectory insert in (a) is not to scale. Cometary ions were first detected on 10 Sep 1985 at ~1500 UT at a distance of $\sim 1.5 \times 10^6$ km from the nucleus [(a)--Ipavich, 1986; (b)--Daly, 1986].

effects in the plasma, yet many features observed in ion data are satisfactorily explained.

Chapter III

A COMET MODEL

Precise ion trajectory calculations require an accurate model of the plasma and magnetic fields which surround a comet. A cometary environment is an extremely complex medium in which to attempt numerical simulations. For example, the size scales range over many orders of magnitude as one goes from the nucleus through the inner coma and the expected contact surface (boundary separating solar wind plasma and cometary plasma--similar to Venus-type ionopause) into the outer coma, the shock front and the extended hydrogen corona (Figure 4)

Various physical and chemical processes which determine the evaporation of volatiles from the surface of the nucleus, the interaction of the neutrals with dust grains, the formation of ions and their interaction with the solar wind are illustrated in Figure 5

Yet despite the vast complexity of the regions around a comet, numerical predictions are proving surprisingly accurate. Multidimensional simulation codes have the unique ability to simultaneously generate plasma and field data on a global scale, which allows tracing of cause and effect relationships. Global simulations are the logical outgrowth of the earlier one-dimensional simulation models (Cravens, 1986). These global simulations are useful for

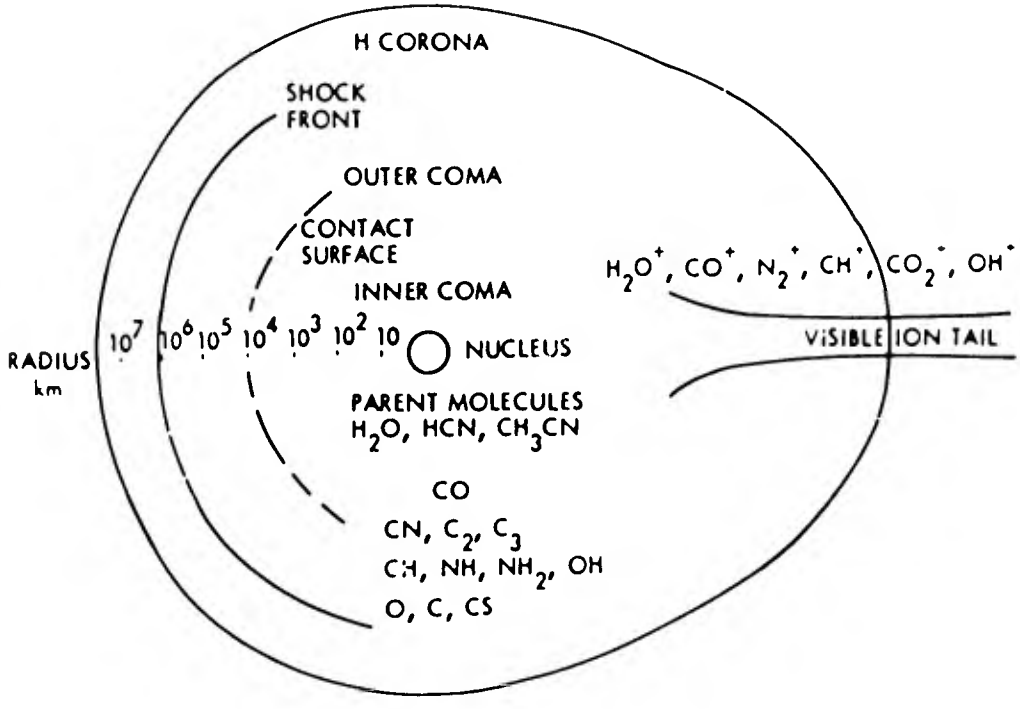

Figure 4. Dimensions of comet-solar wind interaction (Kömle, 1986). Test particles in this simulation are launched at distances up to $\sim 10^6$ km.

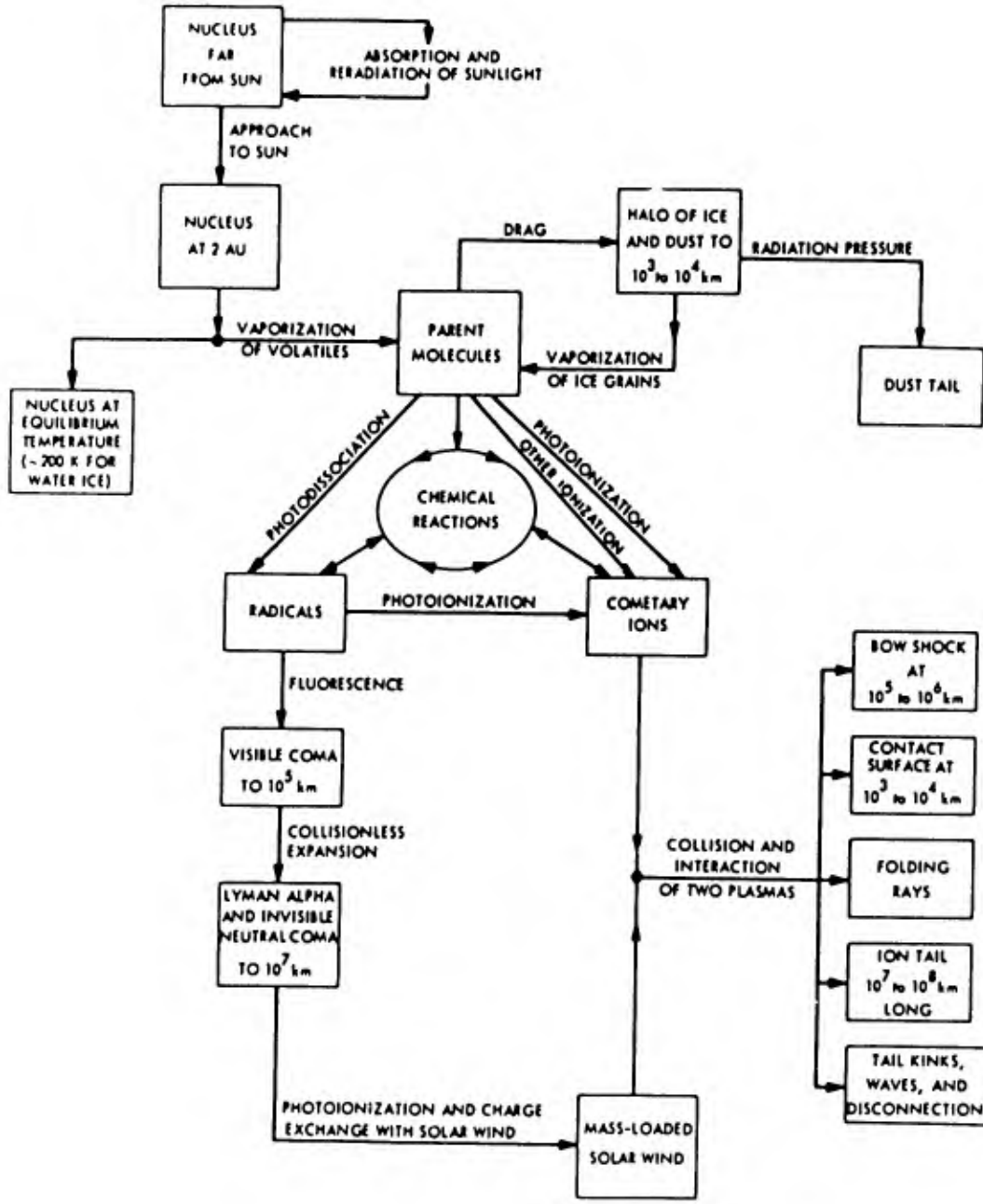

Figure 5. Diagram of various physical, chemical, and radiative transfer processes in a comet (Kömle, 1986).

understanding the data collected by satellites such as ICE and planning future spacecraft missions.

The global MHD model used in this project was developed by J.A. Fedder and co-workers from the Naval Research Laboratory (Fedder et al., 1986), using the multidimensional magnetohydrodynamic (MHD) equations describing a source of particles in a flowing plasma. The basic equations that they solved are the conservation laws for mass, momentum, energy, and magnetic field. The equations are:

Continuity

$$\frac{\partial \rho}{\partial t} = -\nabla \bullet \rho \underline{V} + \sigma N$$

Momentum

$$\frac{\partial \rho \underline{V}}{\partial t} = -(\underline{V} \bullet \nabla)\underline{V} - (\frac{1}{\rho})[\nabla(P + Q) + \underline{B} \times \frac{\underline{J}}{c}] - (\sigma N/\rho)\underline{V}$$

Pressure

$$\frac{\partial P}{\partial t} = -\nabla \bullet P\underline{V} - (\gamma - 1)(P + Q)\nabla \bullet \underline{V} + [(\gamma - 1)/2]\sigma N\underline{V}^2$$

Faraday's Law

$$\frac{\partial \underline{B}}{\partial t} = -c\nabla \times \underline{E}$$

Ampere's Law

$$\underline{J} = c\nabla \times \underline{B}/4\pi$$

Ohm's Law

$$\underline{E} + \underline{V} \times \frac{\underline{B}}{c} = 0$$

where

ρ is the plasma density

$\underline{V}$ is the flow velocity

P is the pressure

$\underline{E}$ is the electric field

$\underline{B}$ is the magnetic field

$\underline{J}$ is the current density

c is the speed of light

γ is the ratio of specific heats

σ is the ionization rate

N is the number density of neutrals, and

Q is an artificial viscosity used to conserve energy in the plasma

The source term represents the production, by photoionization, of cometary ions from the radially expanding cloud of cometary neutrals. The number density of the radially expanding neutrals is given by:

$$N = (mG/\omega R^2) \exp(-\sigma R/\omega)$$

where

m is the mean molecular mass

G is the gas production rate

ω is the expansion velocity

R is the radius from the nucleus, and

σ is the ionization rate

Since the primary ion component is H_2O with smaller amounts of CO_2 and other constituents, a mean molecule mass of 20 amu is used in their simulation. An estimate of the gas production rate of Comet Giacobini-Zinner is 2.3×10^{28} molecules per second (Yeomans and Brandt, 1985). The comet is assumed to have no intrinsic magnetic field.

Solar wind parameters at approximately 0.5 AU were chosen: a speed of 400 km s^{-1}, a plasma density of 8 amu cm^{-3}, a temperature of 5 eV, and an interplanetary magnetic field strength of 7 nT. The simulation box is a Cartesian mesh (29x21x21) with the nucleus located at (12,11,11). The positive x axis points antisunward and extends from 100,000 km upwind of the nucleus to 500,000 km downwind. The z axis is aligned with the undisturbed IMF and extends 100,000 km to either side. The y axis is aligned perpendicular to the z axis. The simulation is carried forward in time for steady solar wind conditions until a quasi-steady state exists throughout the mesh. The model calculates the fluid variables, including the mass density, the thermal pressure, the bulk density, and the vector magnetic field at each point in the grid. These results constitute a prediction of the plasma properties of a comet and its MHD interaction with the solar wind.

The Lorentz force on the cometary ions is computed from the magnetic field ($\underline{B}$) and the plasma bulk velocity ($\underline{V}$), since the convection electric field is

given by $\underline{E} = -\underline{V} \times \underline{B}$. Between the grid mesh points, values of $\underline{V}$ and $\underline{B}$ are obtained from interpolation of the data.

In spite of the observed turbulent nature of the magnetic field and plasma velocity, this model for the ion pick-up calculations is justified from comparison of the simulation results with the observed average behavior of these quantities (Boice et al., 1986; Zwickl et al., 1986). Although the level of fluctuations in the field and flow data along the ICE spacecraft trajectory is high, the background measurements are roughly consistent with the model. By modifying Fedder's MHD model to include fluctuations in $\underline{E}$ and $\underline{V}$, an uncertainty is introduced related to the nature of this perturbation in $\underline{E}$ and $\underline{V}$. These complications, from the introduction of a little-known and inaccurate large-scale turbulence factor, are minimized by considering only the global structure of the field and flow on the analysis of particle behavior.

The behavior of the bulk plasma velocity and magnetic field lines in the model is illustrated in Figure 6. Note that the solar wind streamlines are deflected only slightly by the comet while the magnetic field lines are heavily draped about the comet. This draping of field lines is due to mass loading of the solar wind and the MHD frozen in approximation (infinite conductivity). The effects of magnetic field draping and the MHD approximation cause the comet-solar wind interaction to depart from cylindrical symmetry, as illustrated in Figures 7-10. Velocity contours in the plane of the interplanetary magnetic field (Figure 7) and in the orthogonal plane (Figure 8--looking down on the comet-sun plane) clearly show the nonsymmetric nature of the slowing of the solar wind bulk velocity near the comet due to mass loading. Similar

asymmetry is apparent in the magnetic field compression and draping as shown in Figures 9 and 10.

Despite the vast length scales, formidable complexity and lack of symmetry of the comet-solar wind interaction, there is a general agreement between the observations and the predictions of the MHD model. Figure 11 compares the bulk velocity of the observations with that of Fedder's MHD model, while the observed and model magnetic fields are illustrated in Figure 12.

This global MHD model of the cometary plasma and magnetic fields is here used as a framework upon which to build particle trajectory calculations. The analysis of test particle trajectories shows the individual behavior of the ions. The combination of the MHD model results of the large-scale flow and magnetic fields with calculations of particle trajectories produces a global picture of ion behavior in a comet, as discussed in the next chapter.

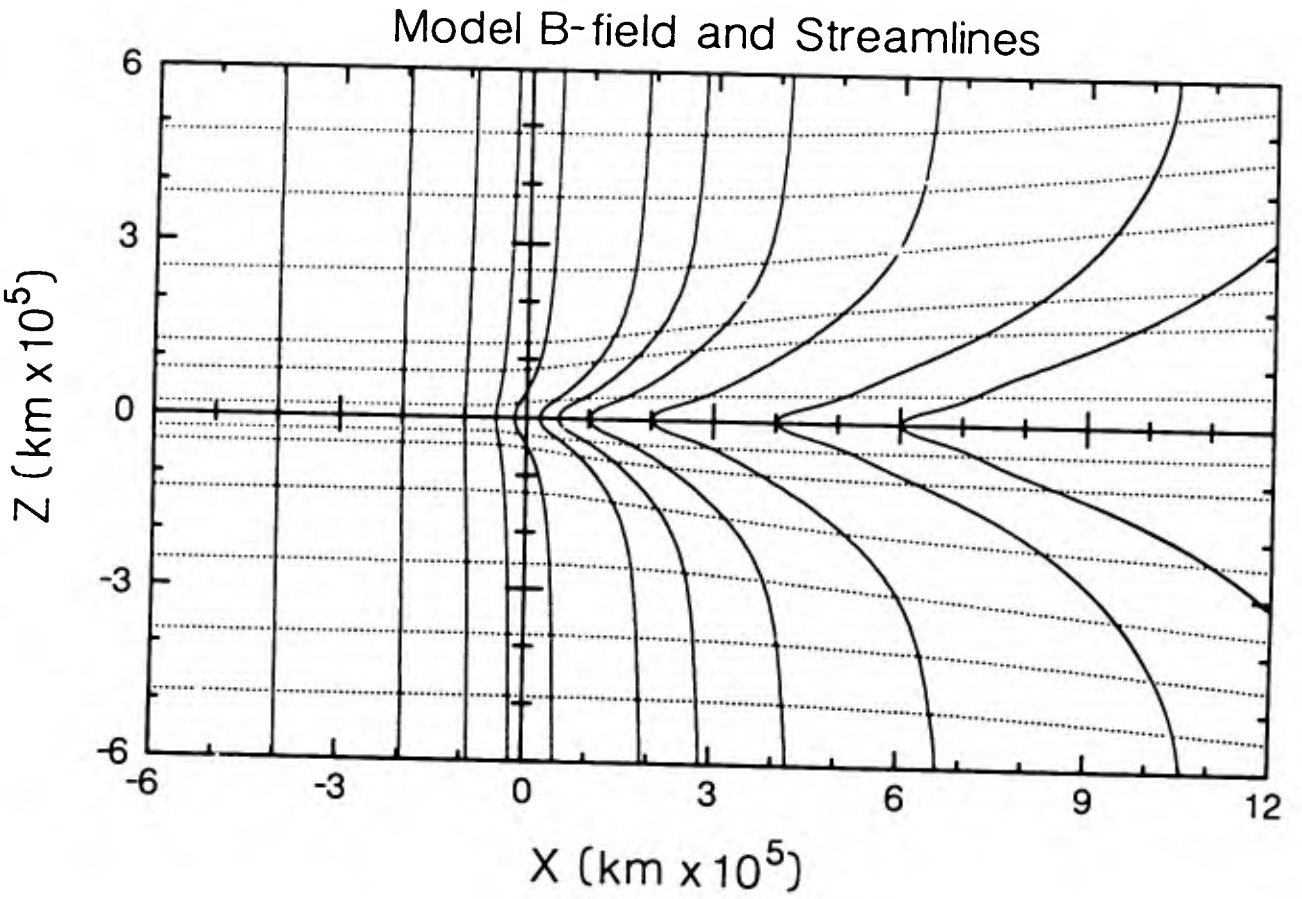

Figure 6. MHD model of Comet Giacobini-Zinner showing magnetic field lines (solid lines) and streamlines (dotted line) in the plane of the IMF. The nucleus is at the origin.

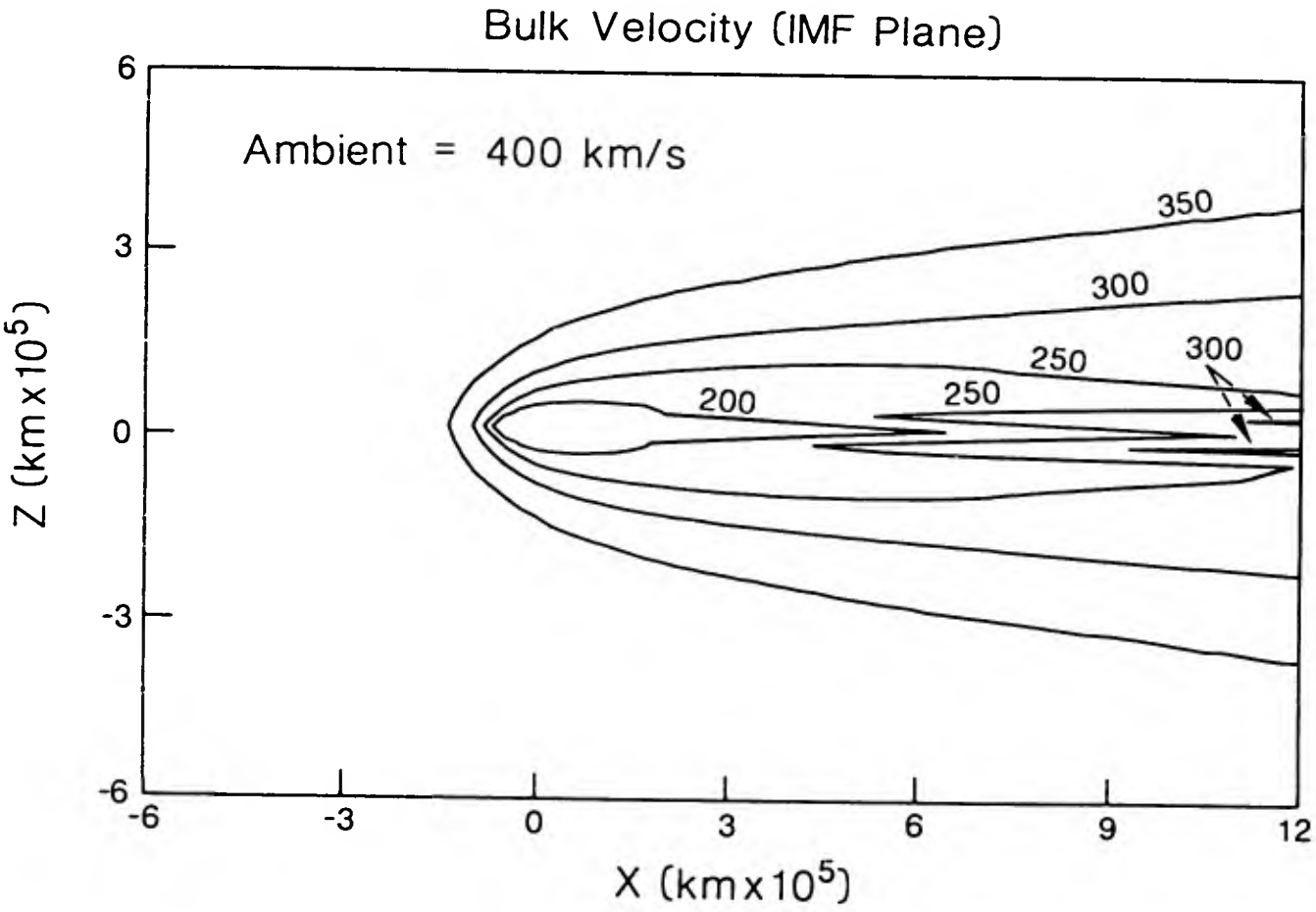

Figure 7. Contours of MHD model bulk plasma velocity in IMF plane.

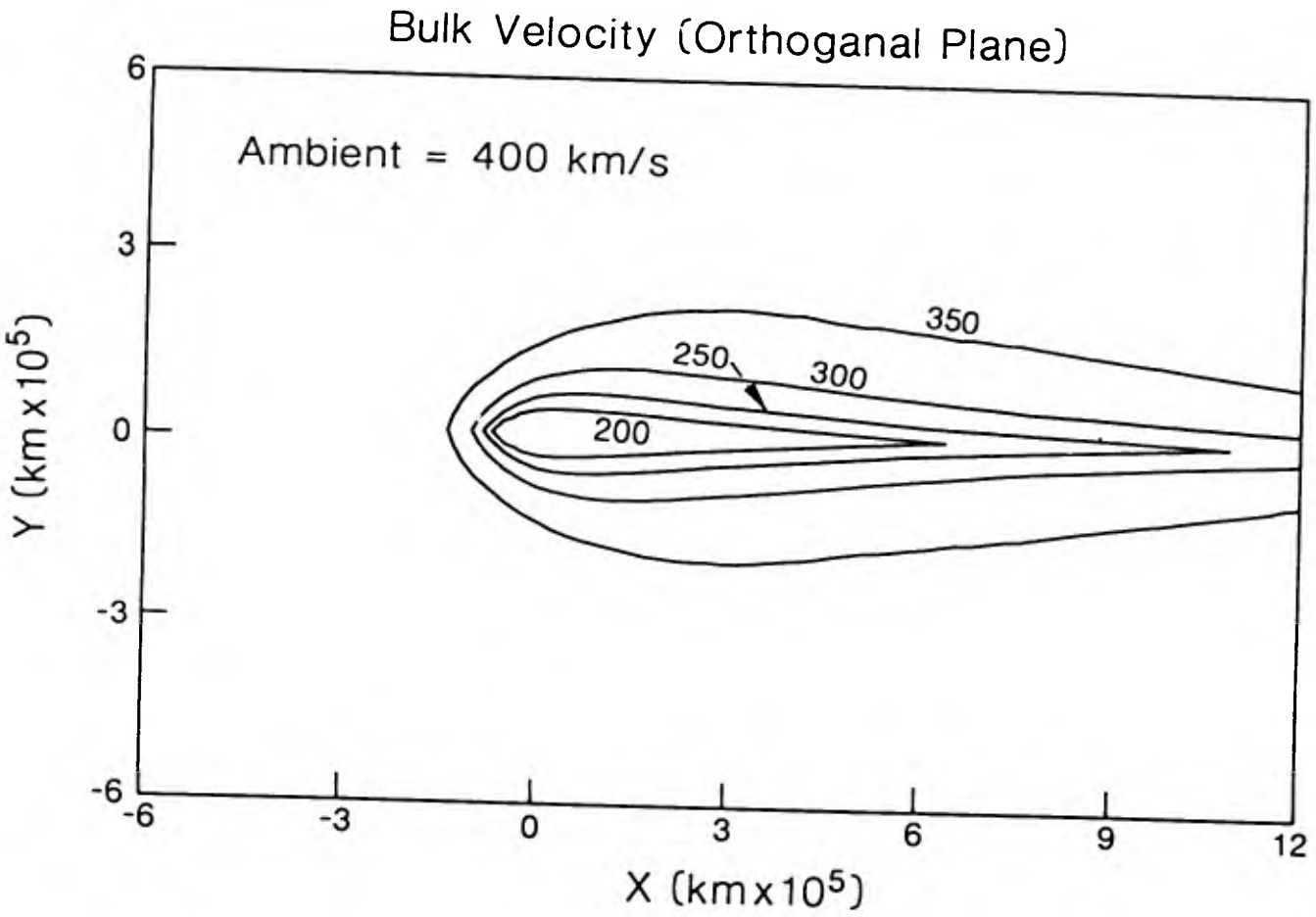

Figure 8. Contours of MHD model bulk plasma velocity in the plane orthogonal to the IMF.

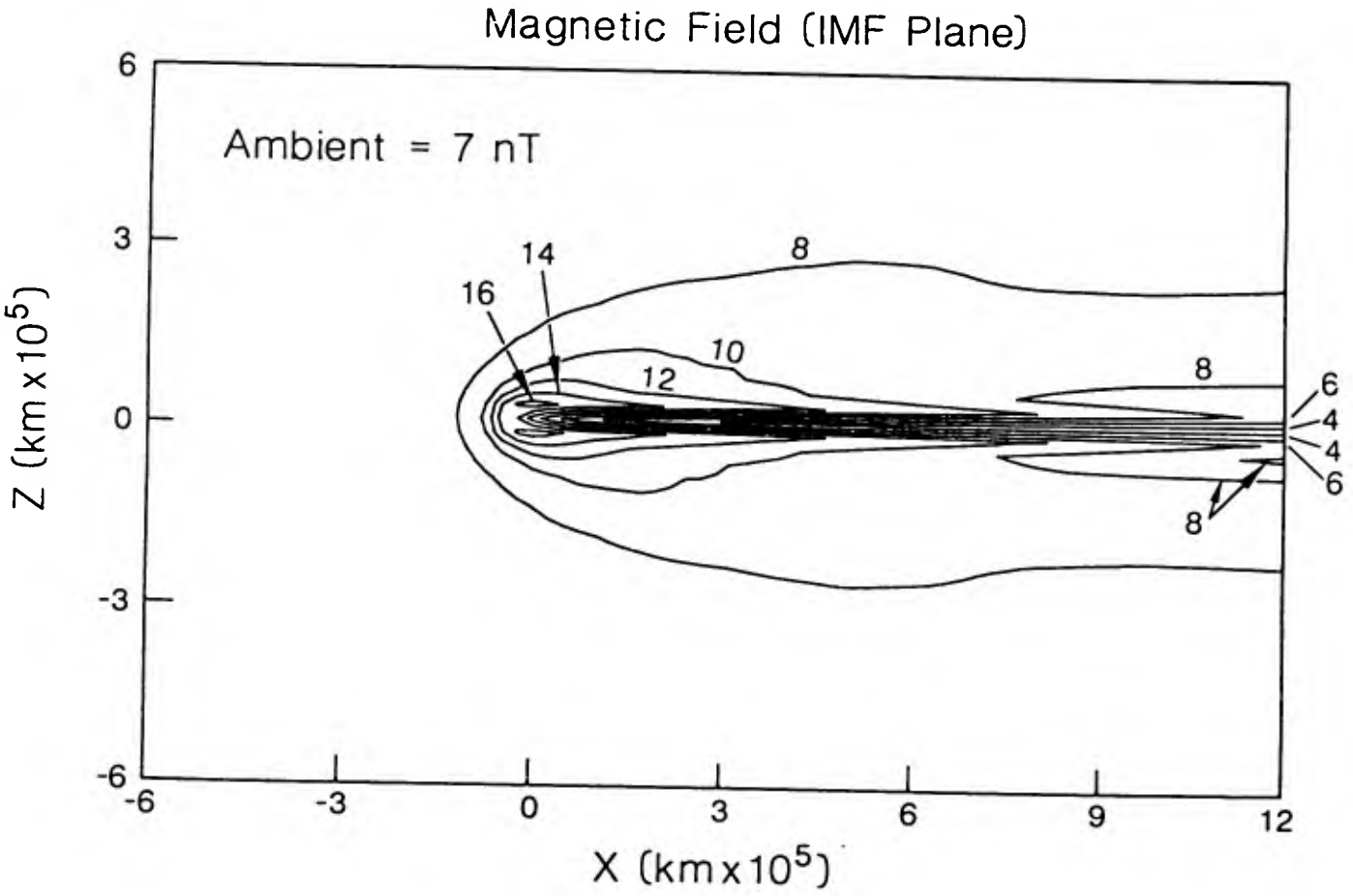

Figure 9. Contours of MHD model magnetic field strength in IMF plane.

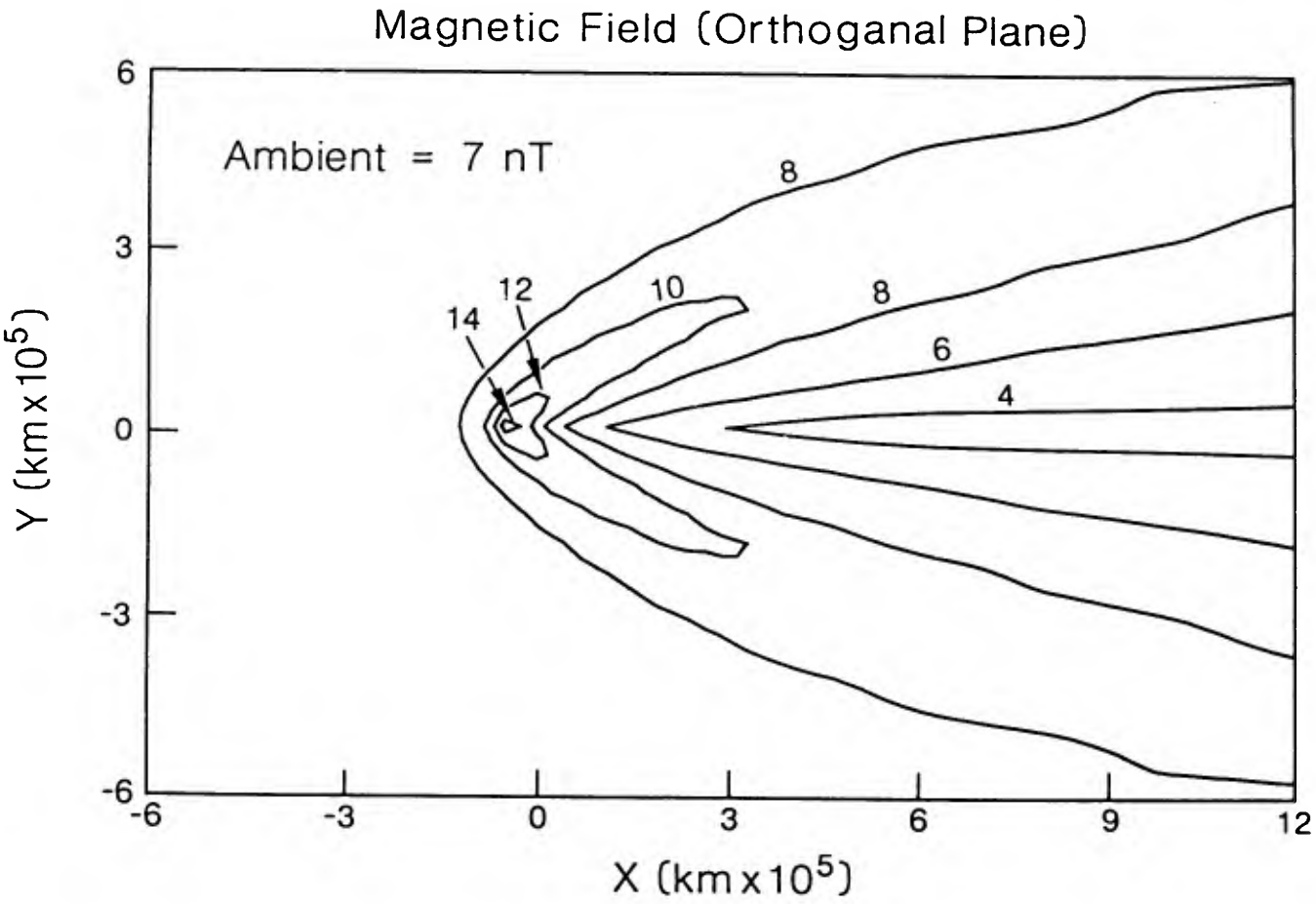

Figure 10. Contours of MHD model magnetic field in plane orthogonal to IMF.

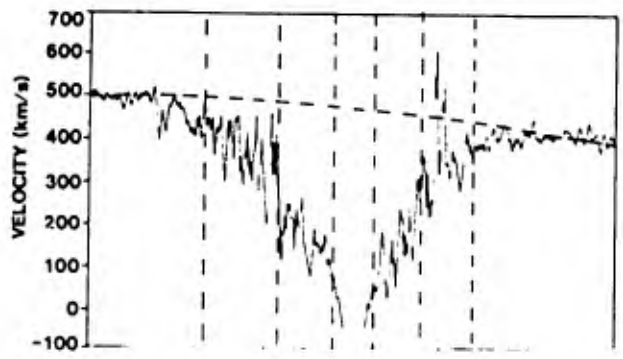

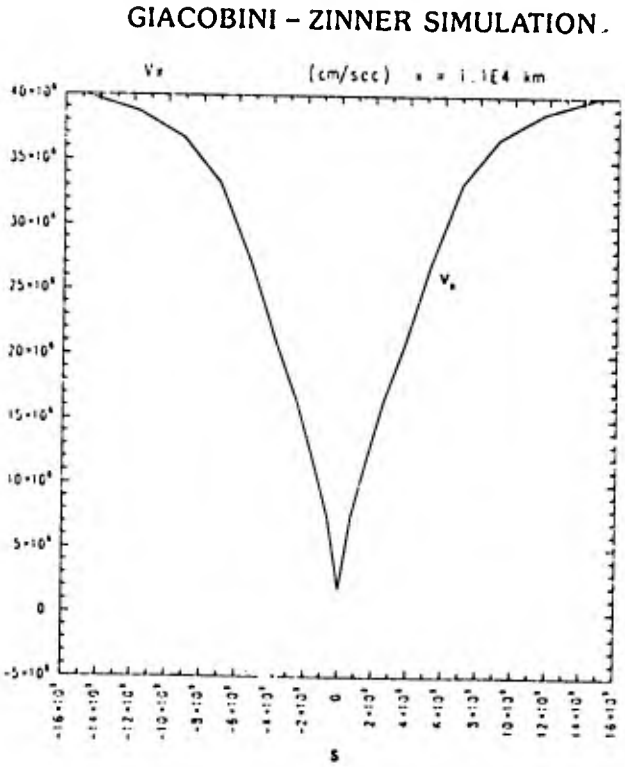

Figure 11. Comparison of observed bulk plasma speed (from Baker et al., 1986) with the MHD model predictions (from Fedder et al., 1986).

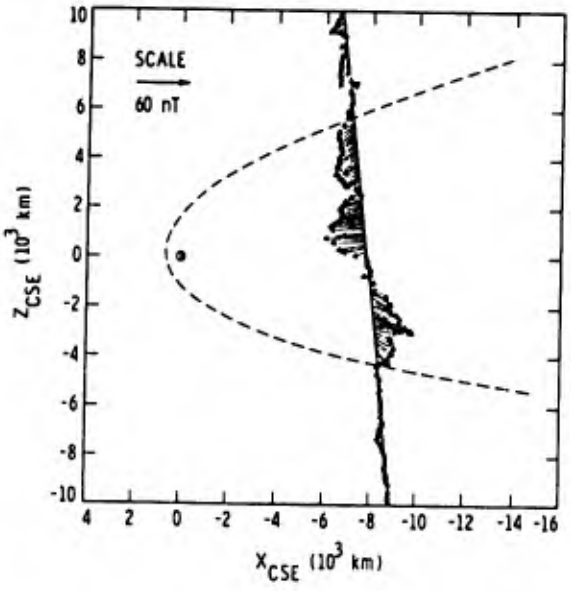

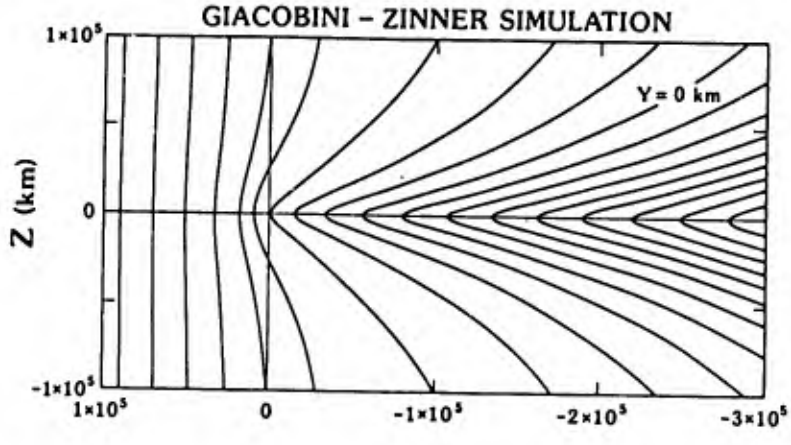

Figure 12. Comparison of observed magnetic field orientation (from Slavin et al., 1986) with the MHD model predictions (from Fedder et al., 1986).

Chapter IV

TEST PARTICLE TRAJECTORIES IN A GLOBAL MHD MODEL

Using the global MHD simulation described in the previous chapter, this study investigates the spatial and velocity space distributions of picked-up energetic ions by injecting a large number of test particles into the simulation and tracing their trajectories. This is the first study to do so in an MHD model, but it is not the first test particle study of cometary ions. Previous test particle studies of cometary ions were carried out by Cravens (1986) and Wallis and Johnstone (1986). In the Cravens study, a large number of ions were examined, but only in a simplified, one-dimensional model of the subsolar coma. The Cravens study provided information on the distribution function of the picked-up ions. Wallis and Johnstone employed an ad hoc draped magnetic field configuration, which they derived by assuming a velocity field that would give the desired magnetic field effect over a large scale. This project uses aspects of both these previous modeling attempts. Like the Cravens study, a large number (750) of cometary ions are used. The initial positions of these ions are radially distributed from the nucleus so as to simulate a realistic ion production function. Like the Wallis and Johnstone study, a three-dimensional model of the large-scale cometary flow and magnetic field environment is used. This combination allows both the microscopic aspects

of the comet (i.e., the cometary particles) and the macroscopic magnetic field and flow structure to be included.

The test particles in this study are actually part of Fedder's original MHD simulation. The Fedder simulation is a single fluid MHD simulation--that is, the cometary plasma and the solar wind plasma are indistinguishable. Thus the two plasma species are treated as a single fluid. The present simulation uses the Fedder model of the background plasma and flow field, but trajectory calculations are performed on individual test particles. Although Fedder does not distinguish between the two species of plasma comprising his single fluid model, the results of the present simulation show that close to the nucleus, practically all of the plasma is of cometary origin, while at great distances from the nucleus, solar wind plasma dominates. By selecting the proper radial density profile of cometary plasma, the present simulation in effect looks at individual cometary ion trajectories.

The starting positions of the ions were placed on the surface of ten concentric spheres with exponentially increasing radii from 0.1×10^5 km to 8.0×10^5 km from the comet nucleus. The 750 starting points (a number selected for computational practicality) were distributed on the spherical surfaces so that the resulting surface densities modeled the radial production function (Schmidt and Wegmann, 1982).

$$P = \frac{Q}{4\pi\tau v_N R^2} \exp\left(\frac{-R}{\tau v_N}\right) \qquad (1)$$

where Q is the number of neutral water molecules released from the comet per second, v_N is the radial speed of the neutral molecules, R is the distance from the nucleus, and τ is the ionization time. The values selected for the variables are in accordance with those from Ipavich (1986): $Q = 3.5 \times 10^{28}$ sec^{-1}, $v_N = 1$ km sec^{-1}, and $\tau = 10^6$ sec. The exponentially increasing radii of the ten starting spheres and the corresponding number of points scattered on the surface of each sphere are displayed in Figure 13. These ten shells of particles are displayed graphically in Figure 14.

In the simulation, the equation of motion $m\ddot{v} = e(\underline{E} + \underline{V} \times \underline{B})$ is solved for ions launched radially with initial velocities of 1 km/s. In the equation of motion, m is the mass of the cometary ion, e is the electron charge, and $\ddot{v}$ is the velocity of the individual ion (in contrast to the bulk velocity $\underline{V}$). A fourth-order Runge-Kutta technique is used to obtain the solution to the equation of motion. Since portions of the particle trajectories are very irregular, the Runge-Kutta technique used here employs an adjustable time step to maintain accuracy. The MHD model, discussed previously, provides values of $\underline{B}$ and the motional electric field $\underline{E} = -\underline{V} \times \underline{B}$ at each location of the particle trajectory. At locations between the computational grid points, interpolation is used to obtain values of $\underline{B}$ and $\underline{V}$. All particles were traced until they leave the MHD model simulation box. Trajectory data, including particle position, velocity, and kinetic energy along with the background flow velocity and magnetic field, were retained for later analysis. Calculations were performed using two different ions: H_2O^+ (18 amu) to illustrate water group ions, which make up most of the mass added to the solar wind by the comet

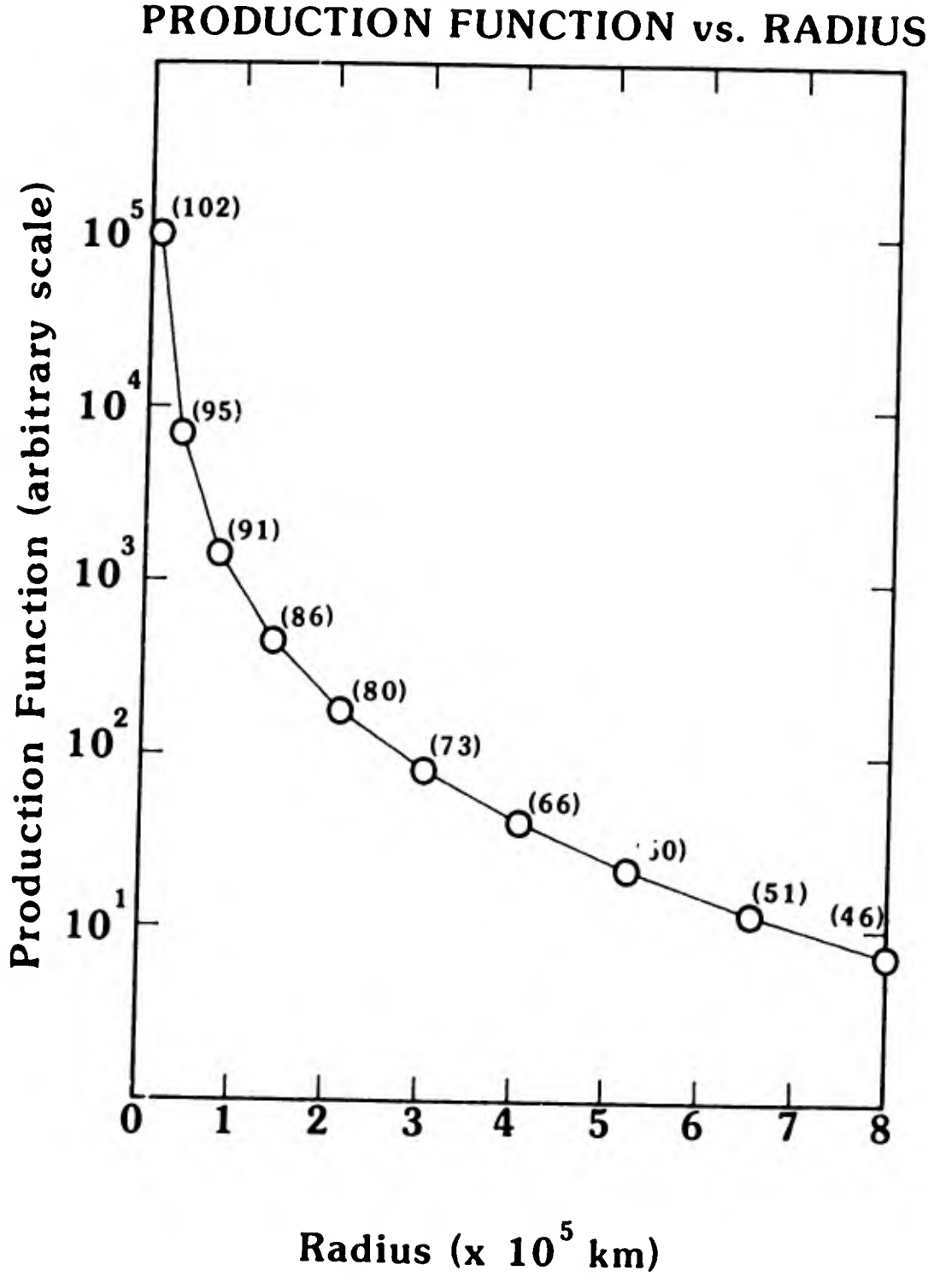

Figure 13. Ion production function vs. radius (see equation 1) showing the number of points initialized on spherical surfaces at each radius (number/$km^2 \propto$ production function).

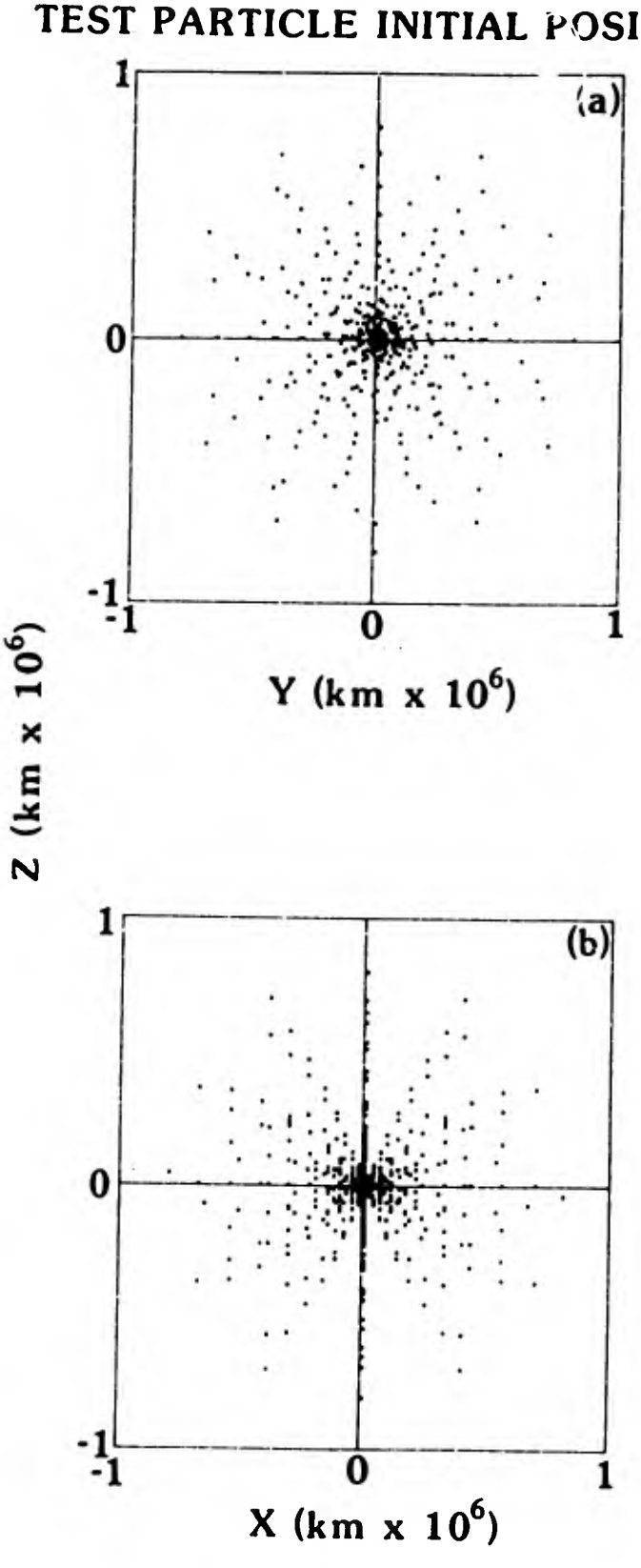

Figure 14. Initial positions of 750 test particles in this simulation along comet-sun axis (a) and in plane of IMF (b).

(Ogilvie et al., 1986), and CO_2^+ (28 amu) to represent the heaviest detected ions.

Projections in the plane containing the interplanetary magnetic field (the x-z plane) of the trajectories of these two ions for three starting grid shells are shown in Figures 15 and 16. These projections most clearly show the two distinctive trajectories that appeared in the earlier results of Wallis and Johnstone (1986). Those particles launched upstream of the outer coma diverge from the tail axis to create a wake of picked-up ions which fan out in the plane of the interplanetary magnetic field. Particles that are initialized at positions close to and tailward of the nucleus generally focus in toward the tail axis where they oscillate between the tail lobes, forming a current sheet in the process. The current sheet feature and two diverging paths away from the tail axis are best seen by looking at points where the particle trajectories intersect planes perpendicular to the x axis at various heliocentric distances. Figure 17 displays some of these "slices" through the simulation box. As anticipated, the formation of a central current sheet composed of cold (low energy) particles along the y axis is evident where the draped interplanetary magnetic field lines are located. In addition, two "wings" of energetic particles are displayed along the z axis, corresponding to the diverging particle trajectories shown in Figures 15 and 16. The trajectory of particles in the plane orthogonal to the plane containing the interplanetary magnetic field is shown in Figure 18. Note that the trajectories show very little divergence in this plane, compared to Figures 15 and 16. The expected cycloidal motion resulting from $\underline{E} \times \underline{B}$ drift is clearly evident in this figure. A final comparison of Figures 15 and 16 shows only an

insignificant difference between H_2O^+ ions and CO_2^+ ions, hence a larger gyroradius. Since this is the only difference between the two ion species, further analysis of particle trajectories will be carried out only on H_2O^+ ions.

Thus the test particle trajectories in the global MHD model yield valuable information about cometary ion behavior. By selecting the particles in accordance with the expected density profile of the cometary atmosphere, the effects of cometary ions are modeled. Both H_2O^+ and CO_2^+ behave similarly with the increased gyroradius due to the larger mass of CO_2^+ being the only notable difference. Particles display two general directions of travel based upon their starting positions in the simulation. Those particles launched into a faster solar wind (upstream of nucleus) diverge from the tail axis, forming two "wings" composed of energetic (>40 keV) particles. Particles launched close to the nucleus in the slower, downstream flow of the solar wind have less energy (<20 keV) and focus into the tail axis, forming the current sheet. The projection of particle trajectories in the orthogonal plane shows characteristic cycloidal motion due to $\underline{E} \times \underline{B}$ drift with very little divergence from the tail axis. These trajectory calculations are the basis for the parameter calculations such as energy spectra, pitch angle distributions, density and velocity profiles that are discussed in the next chapter.

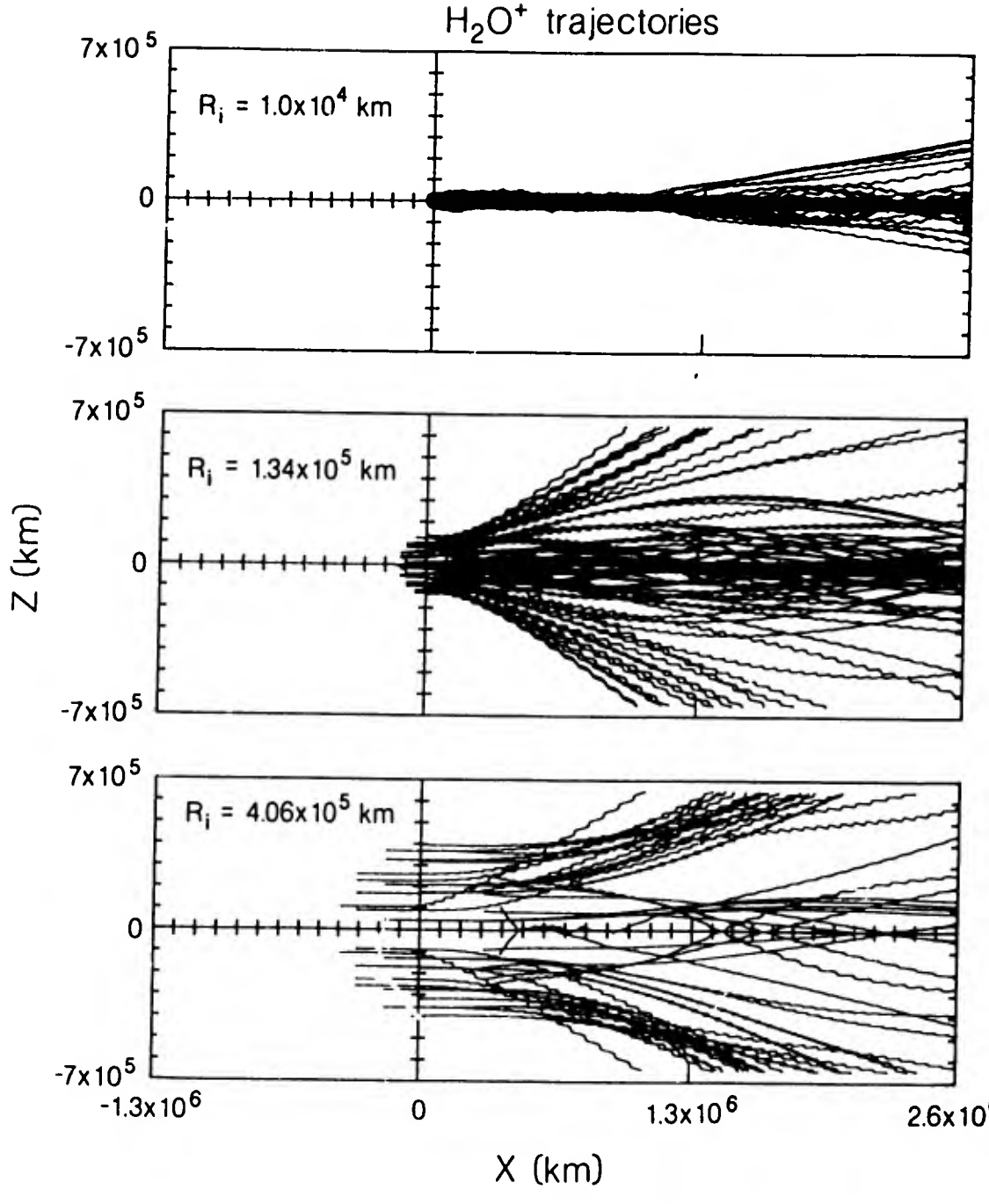

Figure 15. Examples of H_2O^+ test particle trajectories calculated in this study which were launched from an initial radius of R_i with an initial velocity of 1 km/s. Projection is in the same plane as shown in Figure 6 (IMF plane).

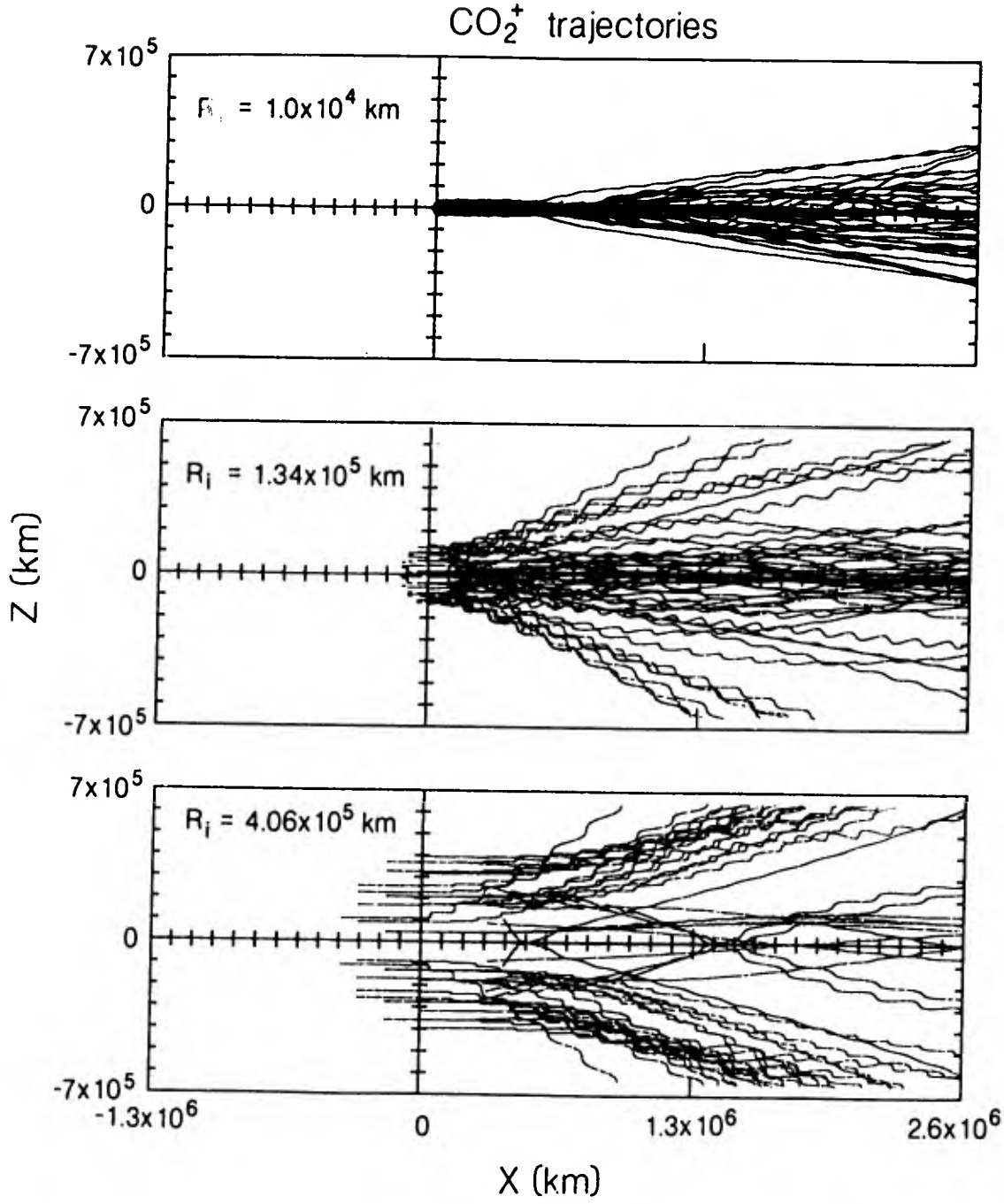

Figure 16. Test particle trajectories for CO_2^+ test particles, otherwise similar to Figure 15.

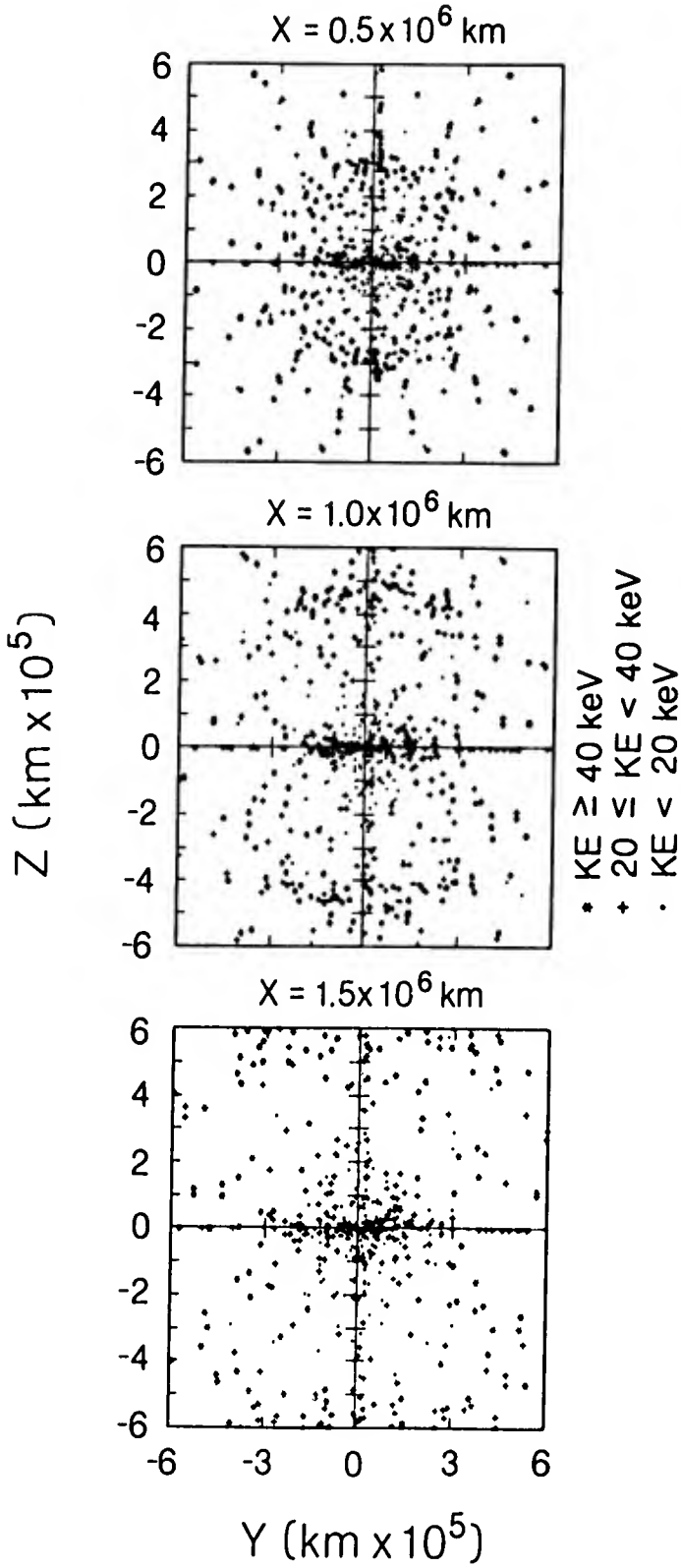

Figure 17. Location and energies of the test particles at increasing distances (x values) downstream of the comet nucleus (in the antisolar direction). Note "cold" plasma sheet along y axis and "hot" wings along z axis.

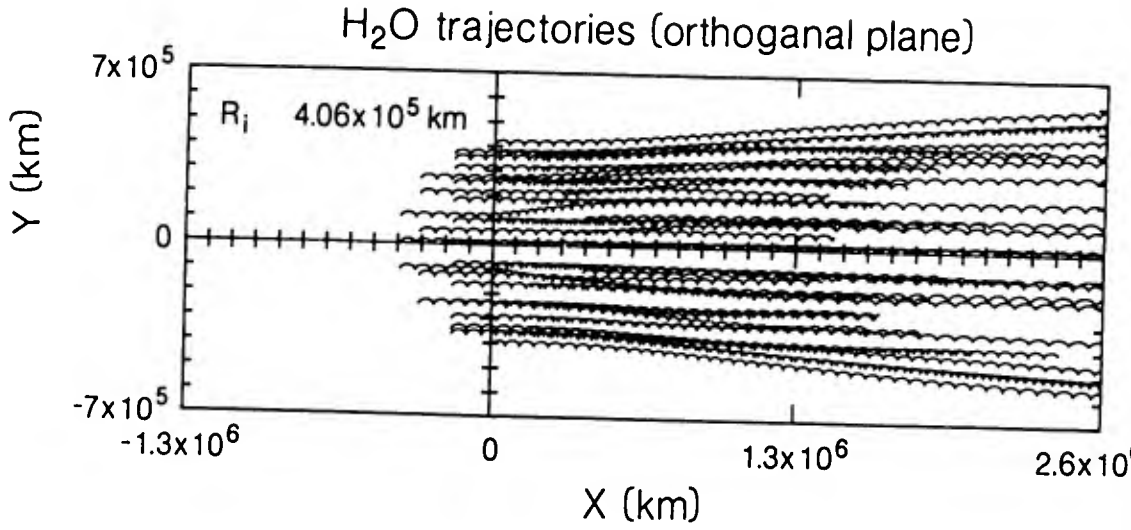

Figure 18. Cycloid motion of H_2O^+ test particle due to $\underline{E} \times \underline{B}$ drift in plane orthogonal to the IMF.

Chapter V

ANALYSIS OF ION TRAJECTORIES

Many analyses of the picked-up ion characteristics can be carried out with the trajectories of the 750 test particles in the simulation described in the previous chapter. The simulation box was first divided into 1×10^5 km-sided cubes to allow statistics to be kept on a relatively small portion of the entire simulation. Five separate properties were then calculated for selected cubes: density profiles, energy spectra, energy profiles, pitch angle distributions, and phase space distributions. By calculating the total time particles spend in a given cube, numbers proportional to the picked-up ion density were obtained Energy spectra and profiles, pitch angle distributions, and phase space distributions were obtained from the particle velocities on entry to a cube. All quantities were calculated in the frame of reference where the nucleus is stationary. Only the results of the analyses of the predominating water group ions are presented below, since both mass groups behave similarly,

To give an overview of the ion population and simulate a spacecraft flythrough, selected "cores" through the simulation box were sampled. These cores, illustrated in Figure 19, were chosen to illustrate variations with both distance from the coma along the comet-sun line and distance from the tail axis in planes parallel and perpendicular to the upstream magnetic field. Since the ICE spacecraft intersected the comet tailward of the nucleus, the present

analyses are restricted to that part of the simulation box downstream of the origin of the coordinates. By adding the total time particles spend in a simulation cube, a pseudo-density profile can be obtained. In Figure 20, these picked-up ion "densities" of the 750 test particles are plotted against the cube sequence number in the core. This figure can be considered a pseudo-time series of density as seen from a spacecraft traveling down the core at a constant speed. A normalization factor must be applied to scale the 750 particles to represent the actual production of 3.5×10^{28} particles per second. Only a few of the density cores are shown because they illustrate the trends in the picked-up ion population. In the core along the comet-sun line (3x), the densities are highest because the ions produced near the nucleus, where the production rate is greatest, focus into this path (see Figures 16 and 17). However, there are secondary maxima in density tailward of the nucleus in cores passing parallel to the tail axis in the plane lying parallel to the upstream magnetic field (1x,2x). The particles that make up these secondary maxima are those which have been picked up in the upstream coma and then deflected away from the tail axis (see Figures 16 and 17). If this latter behavior is the explanation for cometary tail rays (cf. Ip and Axford, 1983), the observed closing and opening of the ray structure could result from the perspective of the observer with respect to the upstream magnetic field as suggested elsewhere.

Kinetic energy spectra along selected cores are shown in Figures 23-26. As mentioned above, these represent statistics of the particle properties on entry into a given cube of the core. Energy bins of 0-1 keV, 1-5 keV, 10-20

Selected Simulation Flythroughs

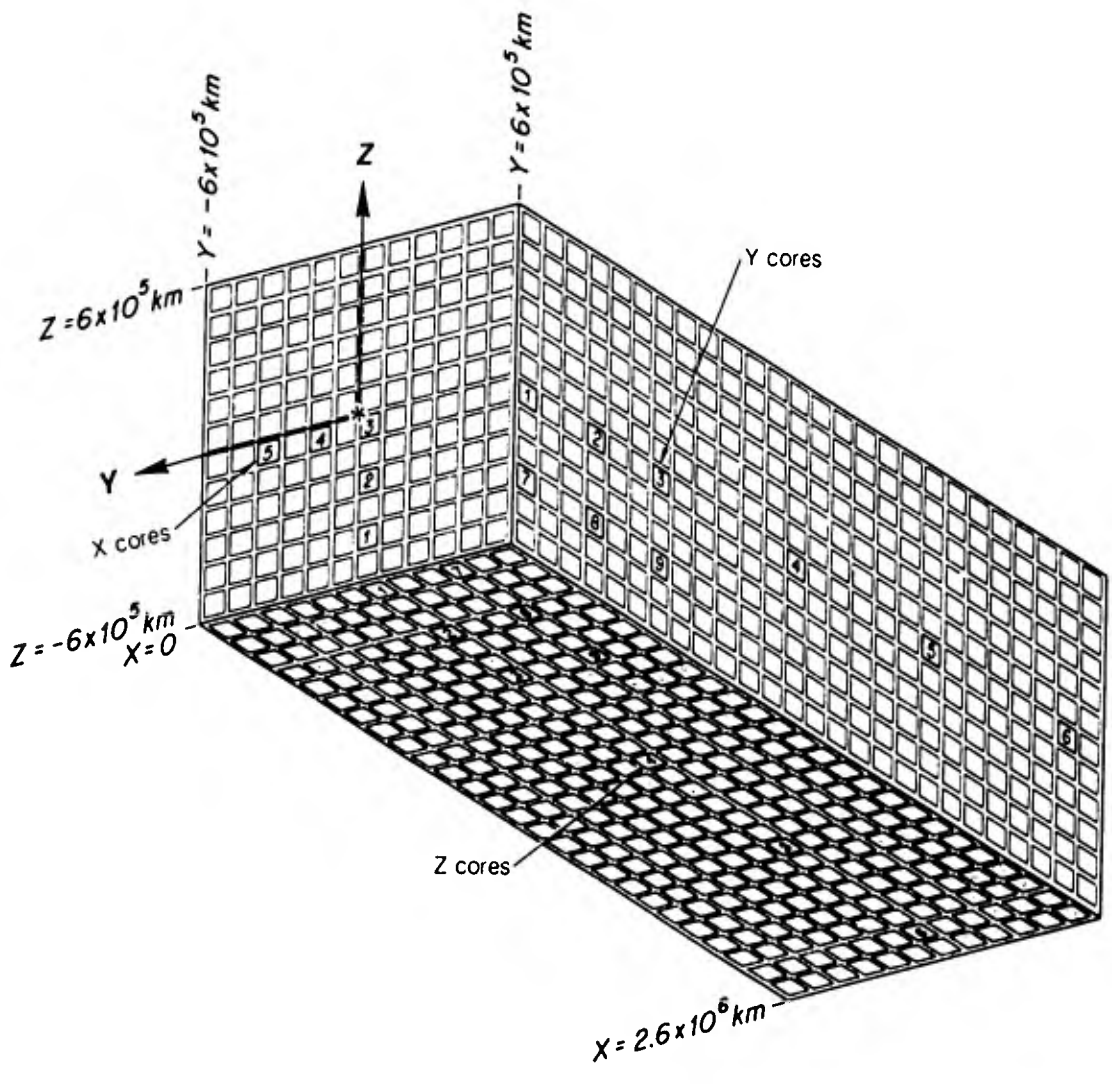

Figure 19. The area of the MHD simulation antisunward of the nucleus (+x direction) divided into 3.744 "cubes" of sides 1×10^5 km. Selected "cores" are numbered for identification and used for trajectory analysis. The comet nucleus is represented by an asterisk.

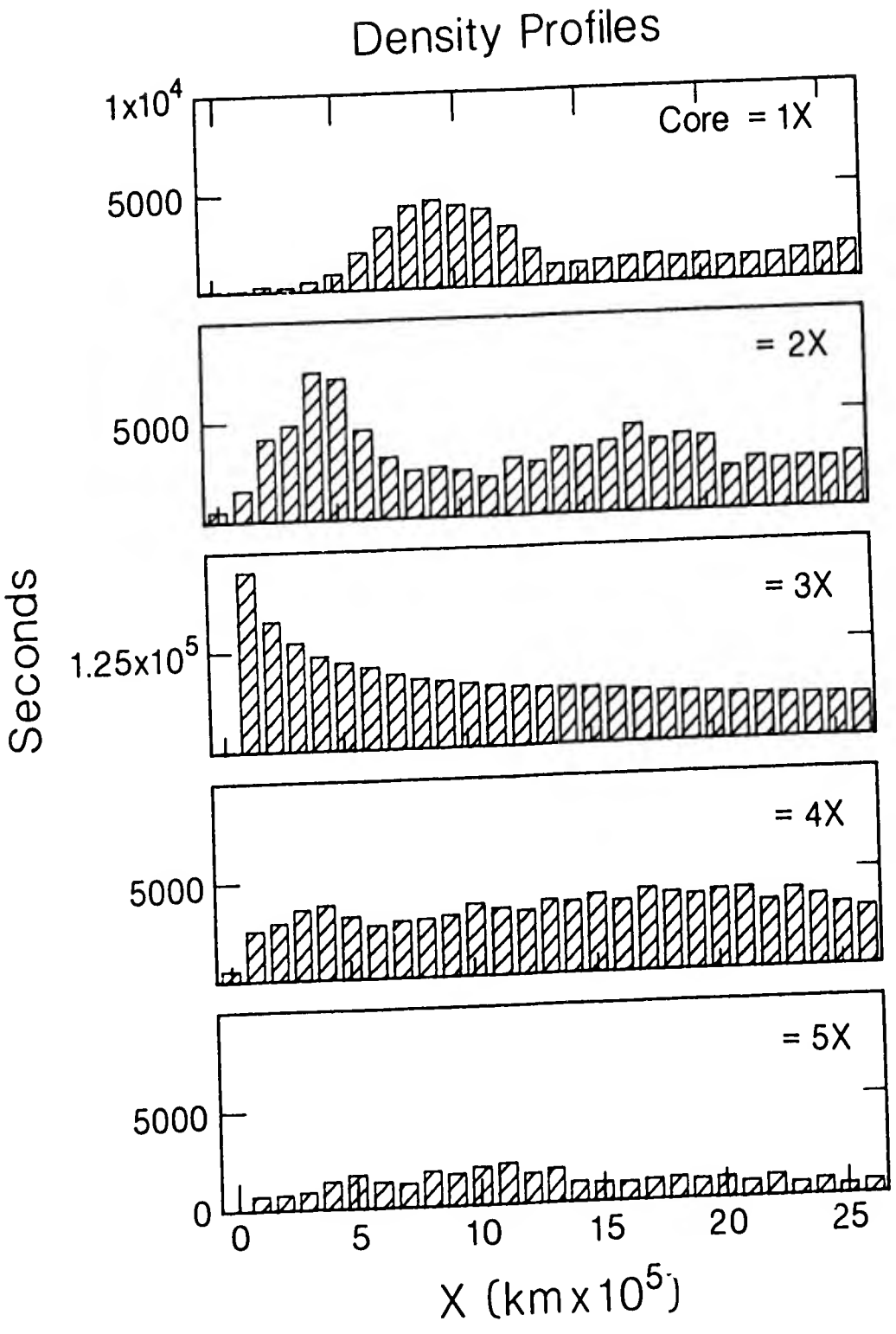

Figure 20. Density profile of test particles in this simulation along the x cores (see Figure 19). Density is proportional to the total time particles spend in each cube. Along the tail axis (Core 3x) densities are 25 times greater than the other other cores, in accordance with Fedder's MHD simulation.

keV, 20-30 keV, 30-40 keV, 40-50 keV, and 50-60 keV were chosen to give statistically significant samples at both the lowest and the highest energies. Each spectrum represents one cube. Looking at the energy spectra from Core 3x, note the very large population of extremely cold ions (0-1 keV) in the first cube (Figure 21), which corresponds to the area directly behind the comet nucleus. Moving off this tail axis core into Core 2x (Figure 22), note the far fewer number of cold ions and an increase in higher energy particle downstream. These higher energy particles move progressively downstream (higher x values) as the distance from the tail axis (Core 3x) increases (Figure 23, Core 1x). In the z-cores, which lie along the direction of the interplanetary magnetic field, Figures 24-26, note that the peak distribution occurs in cube $z=6$, corresponding to the tail axis cores (Figure 21, Core 3x). Close to the nucleus (Figure 24, Core 1z), a significant number of counts appear in cubes adjacent to cube $z=6$. As the distance from the nucleus is increased in Figures 25 and 26, note that the energetic particles fan out in progressively larger distances from the tail axis cube ($x=6$-7). A similar pattern is noted in the y core spectra, although the divergence from the tail axis is not a pronounced as in the z cores (Figures 27-29). These results are particularly relevant to the ICE observations because they show that the low energy and high energy populations behave differently. The ICE experiments were sensitive only to the higher energies. This difference is more apparent when the spectral results are displayed as pseudo-time series. Figures 30-38 show the statistics of the test ions in increasing energy bins along the same selected cores. Here it is seen that, in the plane of the upstream magnetic field, (Figures 33-35), the lower

energy particles tend to monotonically increase as one approaches the tail axis along a orthogonal core. In contrast, the higher energy particles have well-separated maxima to both sides of the tail axis (Figures 34-35).

This separation of high- and low-energy particles due to the background velocity and magnetic field structure is also illustrated in Figure 17. The asterisks, representing high-energy particles (energies above 40 keV) in a particular slice along the x-z plane as shown, make up the two "wings" of the trajectory distributions located a distance away from the tail axis. The lowest energy (below 20 keV) particles, represented by dots, form the expected current sheet which spreads out along the $\pm y$ (in the direction perpendicular to the upstream magnetic field). The plus signs identify the trajectories of intermediate energy (20-40 keV) particles and are located between the high- and low-energy particles.

Pitch angle distributions also reflect the influence of upstream conditions in the magnetic field and velocity structure. Along the tail axis core, Figure 39, which contains primarily the cold particles picked up near the nucleus, shows the distribution centered at 90°, indicating a pancake type distribution. However, the pitch angle distributions from the cores parallel to the tail axis, Figures 40 and 41, are skewed to values between 90° and 180°. These conic distributions are created by the energetic wings of particles diverging from the tail axis. The results of this simulation give a pancake distribution of pitch angle ($\alpha = 90°$) along the tail axis, while the wings of energetic particles produce a conic distribution ($90° < \alpha < 180°$) in cores away from the tail axis.

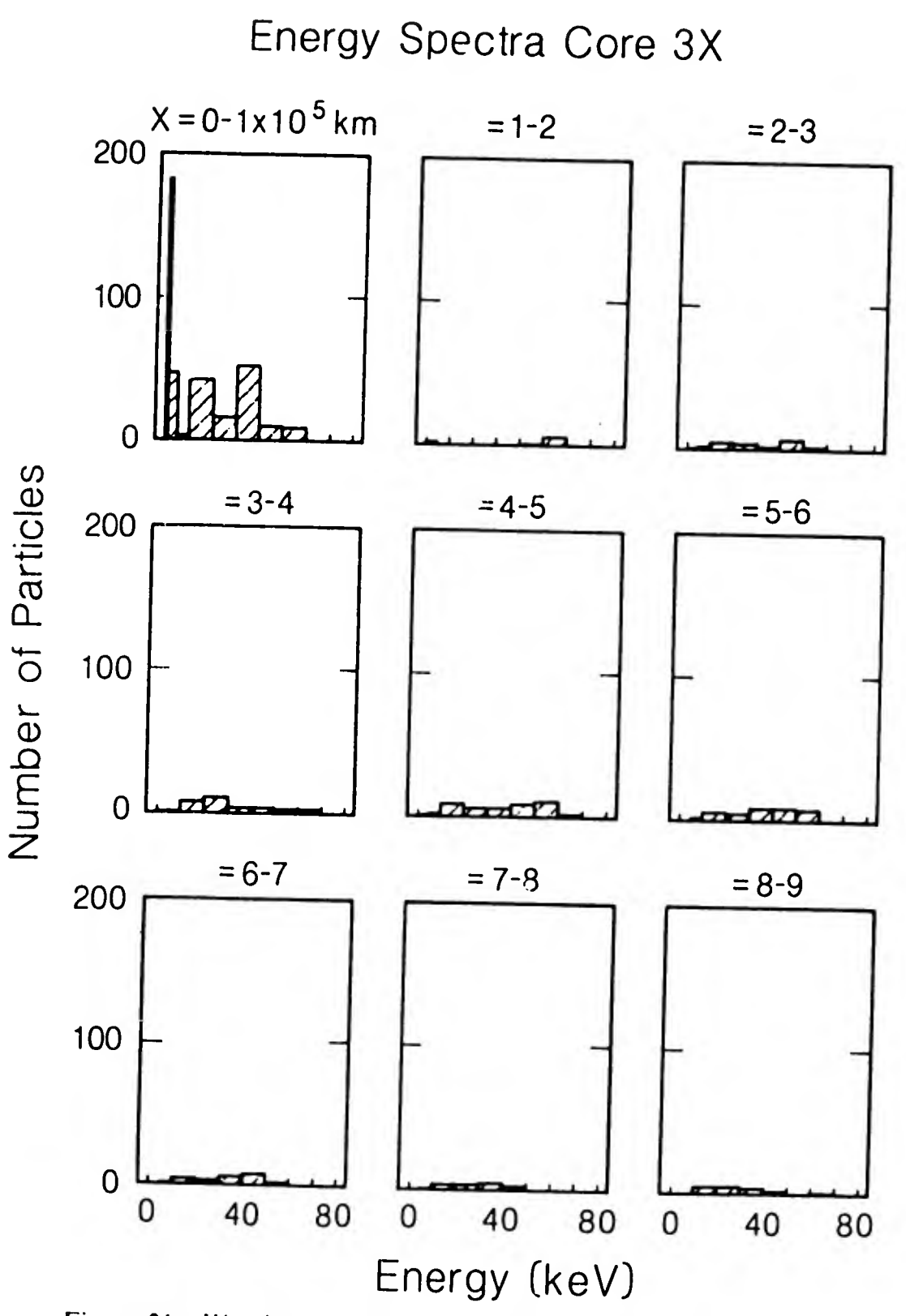

Figure 21. Kinetic energy spectra for the first 9 cubes along the tail axis (Core 3x). The energies are divided into the following ranges (in keV): 0-1, 1-5, 5-10, 10-20, 20-30, 30-40, 40-50, 50-60, 60-70, 70-80. Note large proportion of cold ions in the first cube.

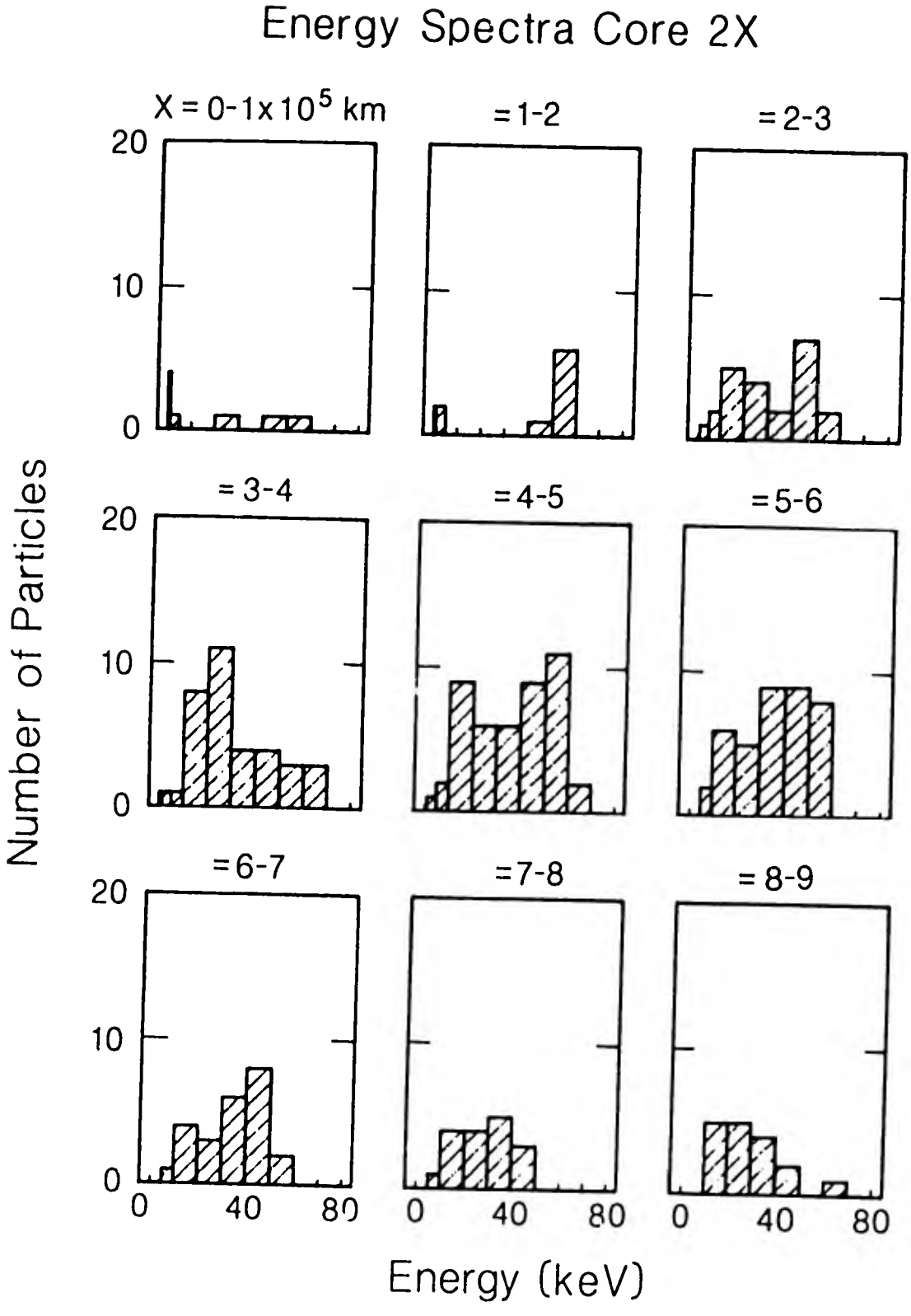

Figure 22. Like Figure 21 for Core 2x (see Figure 19). Core 2x is parallel to the tail axis and displaced 3×10^5 km in the -z direction. Note the scale change between Figures 21 and 22.

Figure 23. Like Figure 21 for Core 1x (see Figure 19). Core 1x is parallel to the tail axis and displaced 5×10^5 km in the -z direction. Same scale as Figure 22. Note particles appear farther downstream than in the previous core.

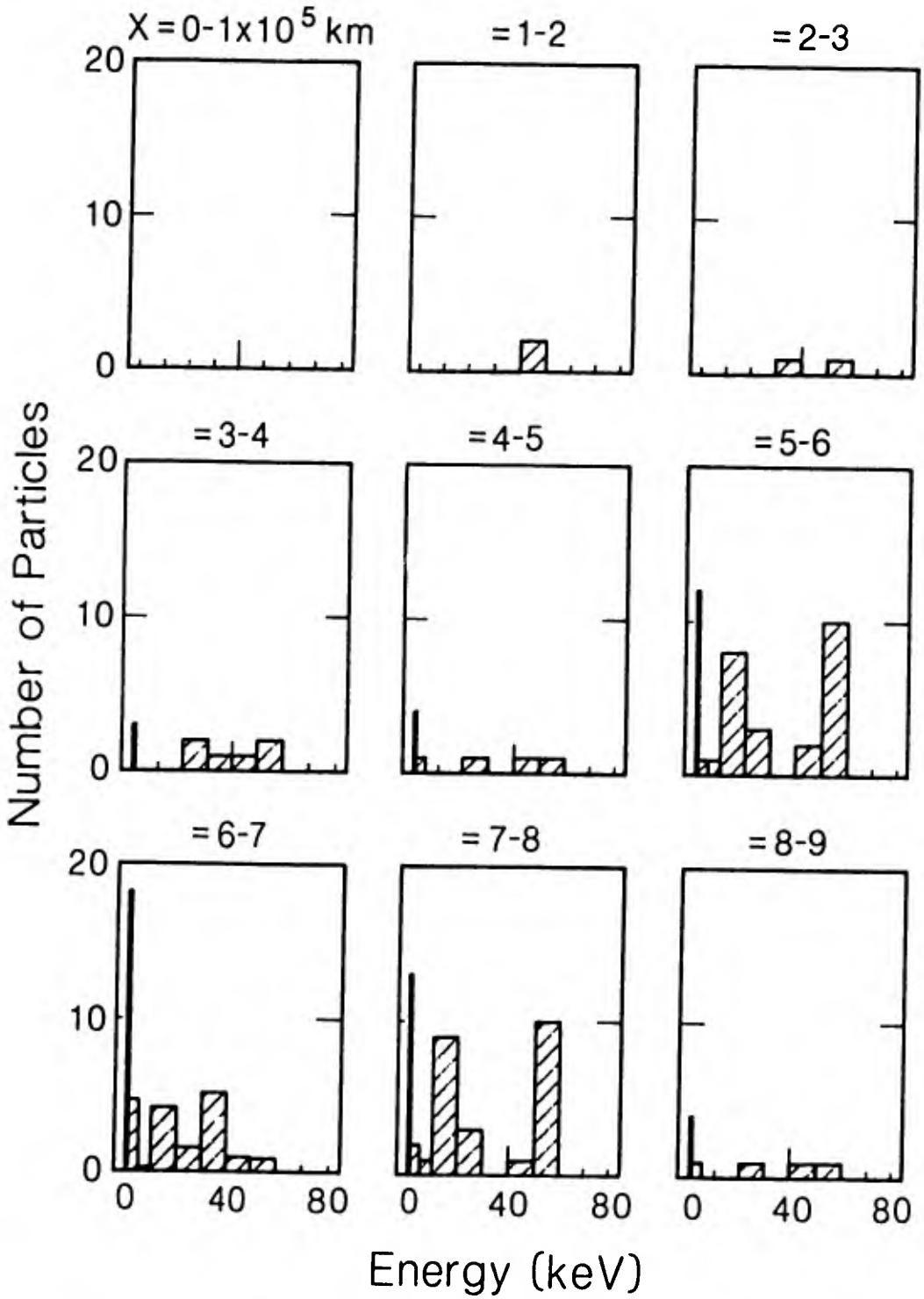

Figure 24. Kinetic energy spectra for the first 9 cubes in Core 1z (see Figure 19). Core 1z is parallel to the z axis, 1×10^5 km antisunward of nucleus, midway through the simulation region in the +y direction. The z cubes are in the plane of the IMF. Note double-peaked distribution in cubes adjacent to tail axis cube (x = 6-7).

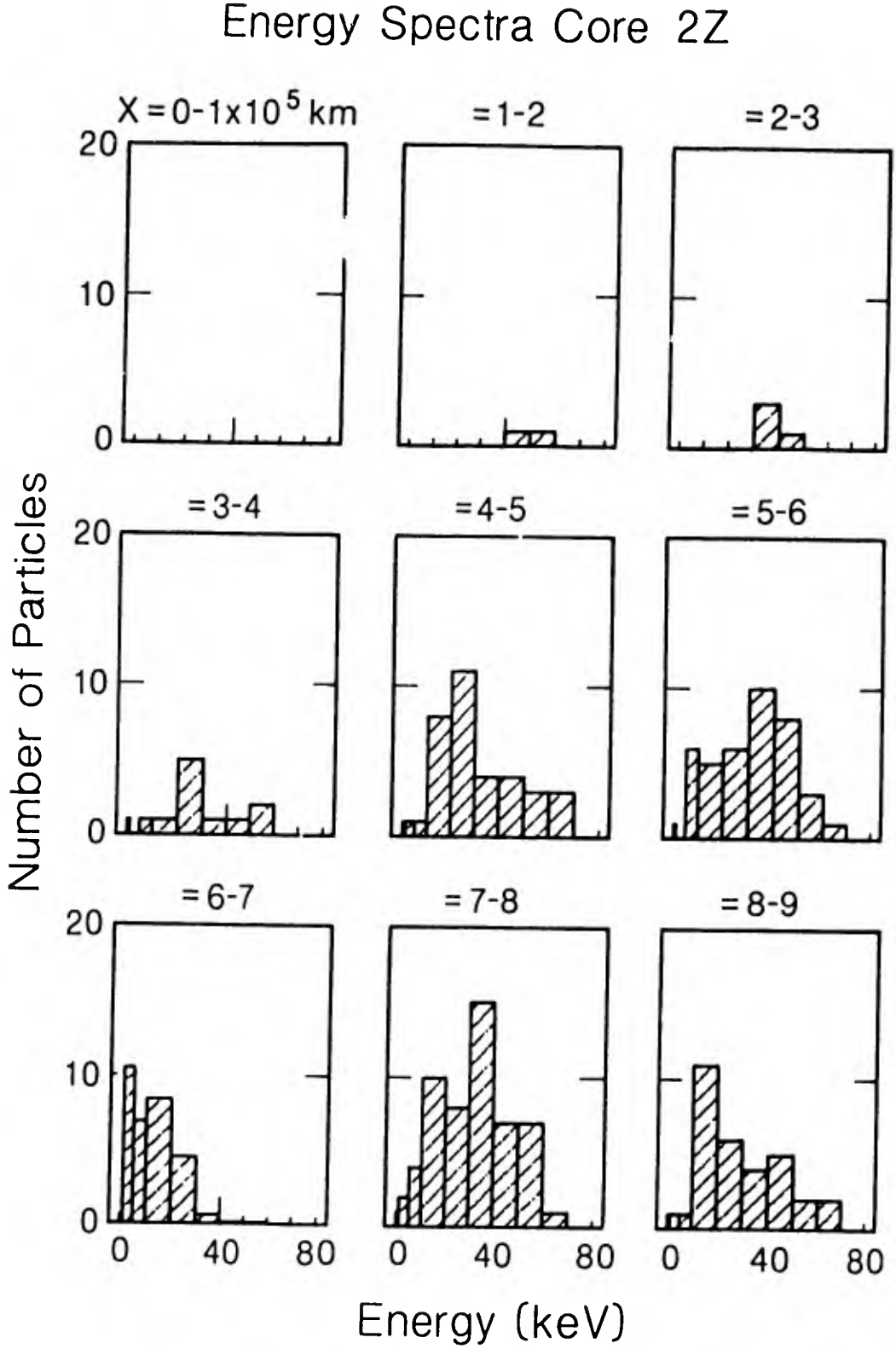

Figure 25. Like Figure 24 for Core 2z (see Figure 19). Core 2z is parallel to the z axis, 4×10^5 km antisunward of nucleus, midway through the simulation region in the +y direction. Particles first appear in cubes farther from tail axis cube than in previous figure.

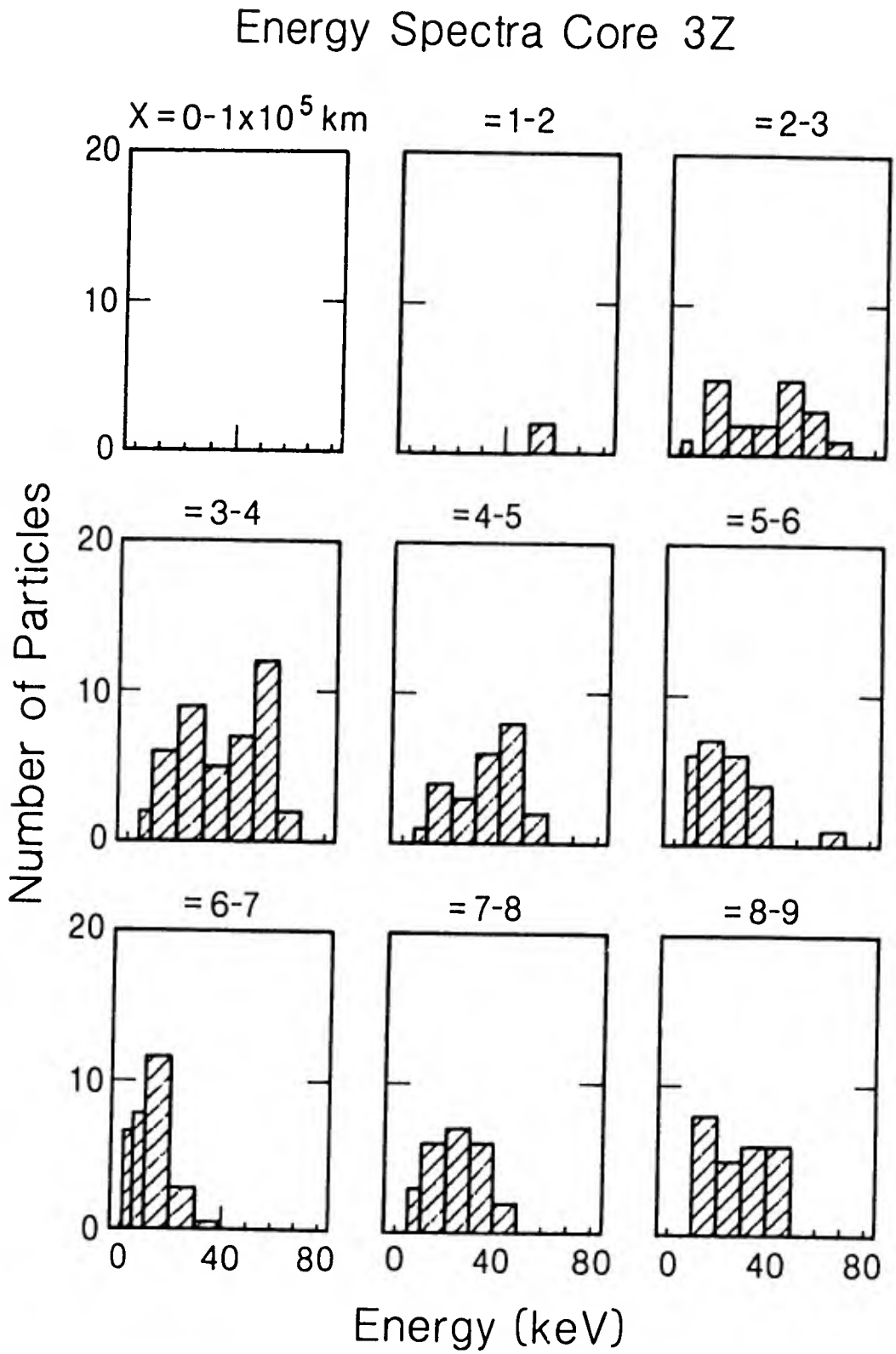

Figure 26. Like Figure 24 for Core 3z (see Figure 19). Core 3z is parallel to the z axis, 7×10^5 km antisunward of nucleus, midway through the simulation region in the +y direction. Progression of particles farther from tail axis cube continues.

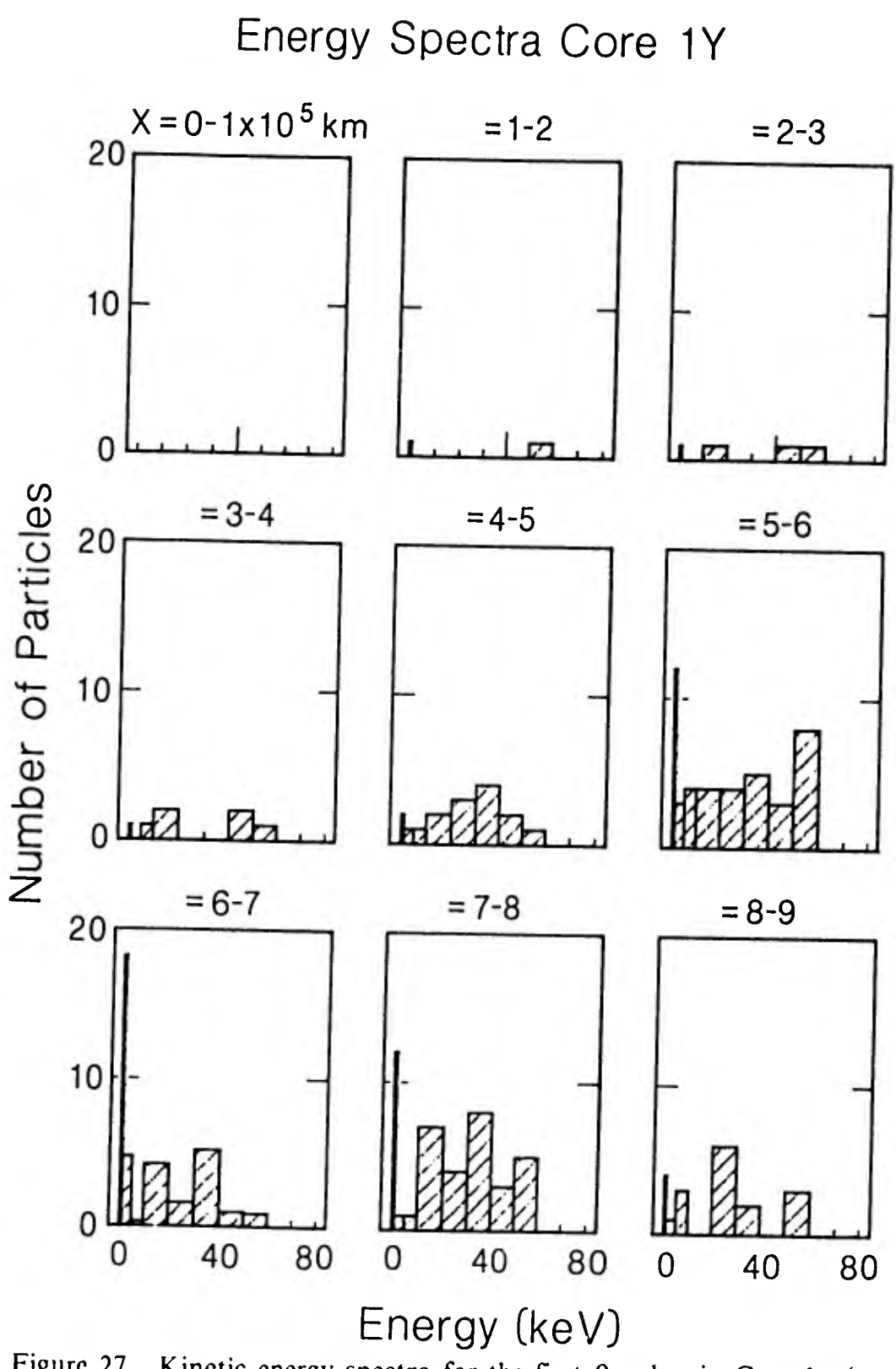

Figure 27. Kinetic energy spectra for the first 9 cubes in Core 1y (see Figure 19). Core 1y is parallel to the y axis, 1×10^5 km antisunward of nucleus, midway through the simulation region in the +z direction. The y cores are in the plane orthogonal to the IMF. Note the double-peaked distribution is not as pronounced as in the z cores.

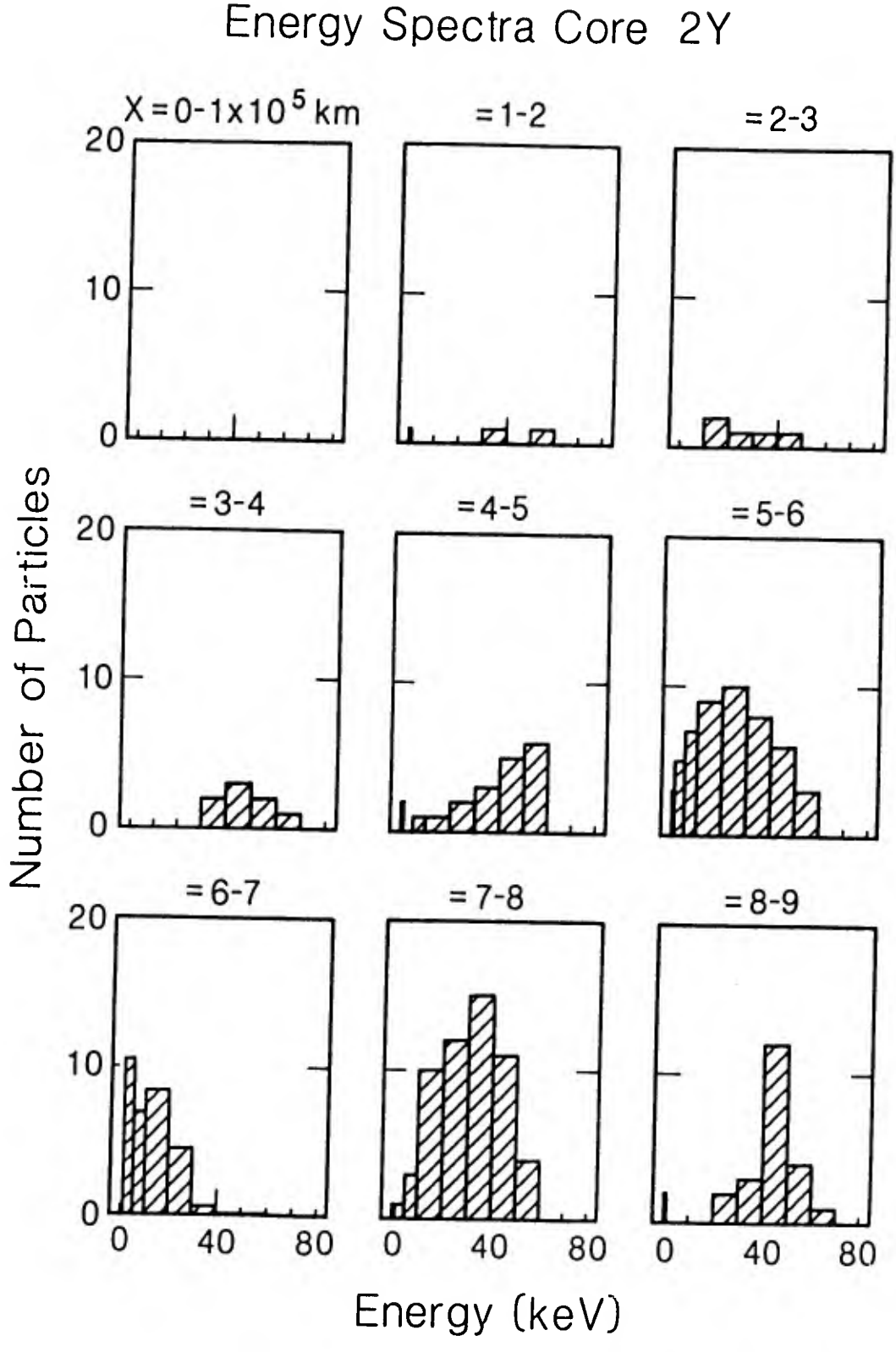

Figure 28. Like Figure 27 for Core 2y (see Figure 19). Core 2y is parallel to the y axis, 4×10^5 km antisunward of nucleus, midway through the simulation region in the +z direction.

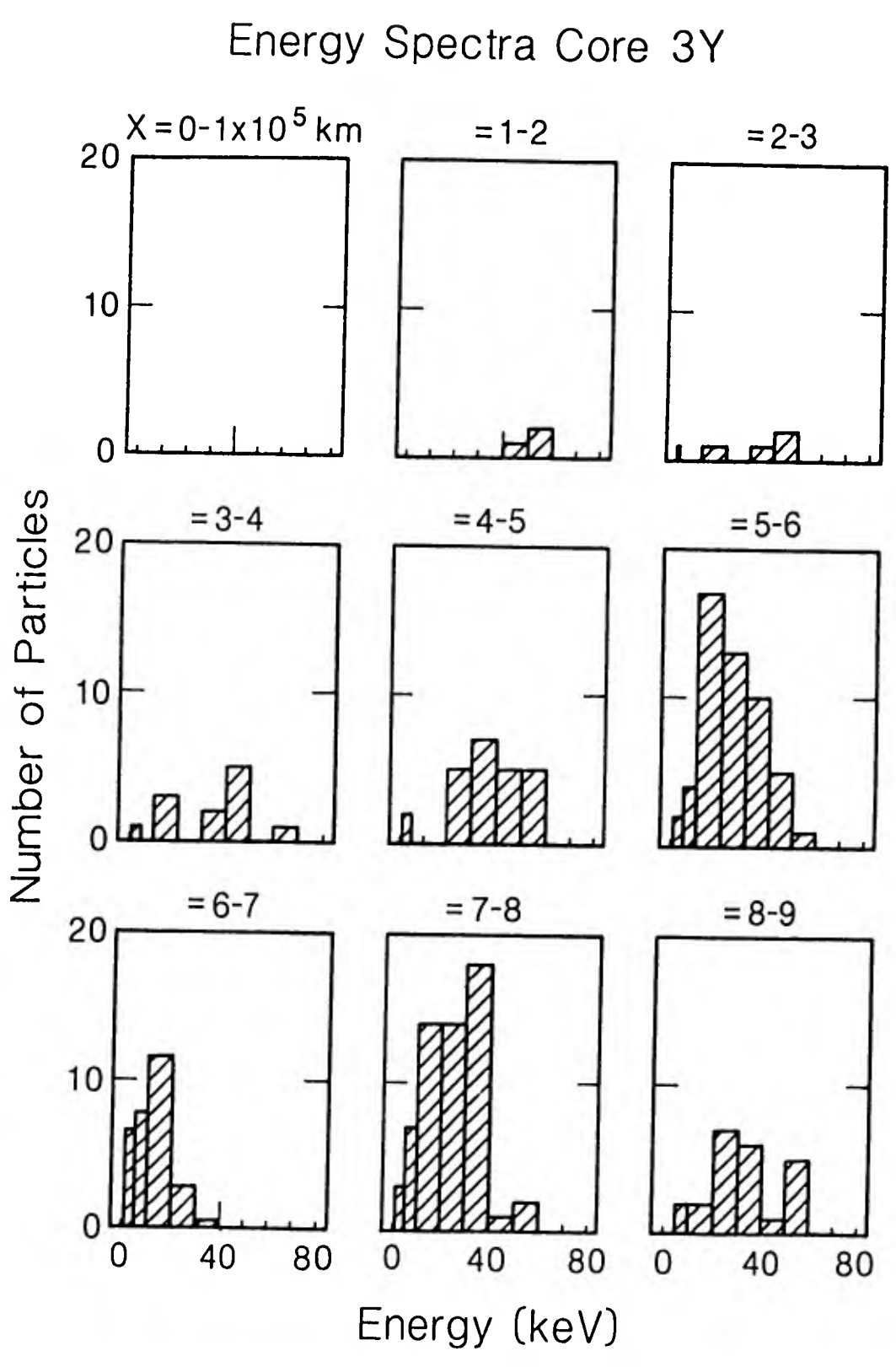

Figure 29. Like Figure 27 for Core 3y (see Figure 19). Core 3y is parallel to the y axis, 7×10^5 km antisunward of nucleus, midway through the simulation region in the +z direction.

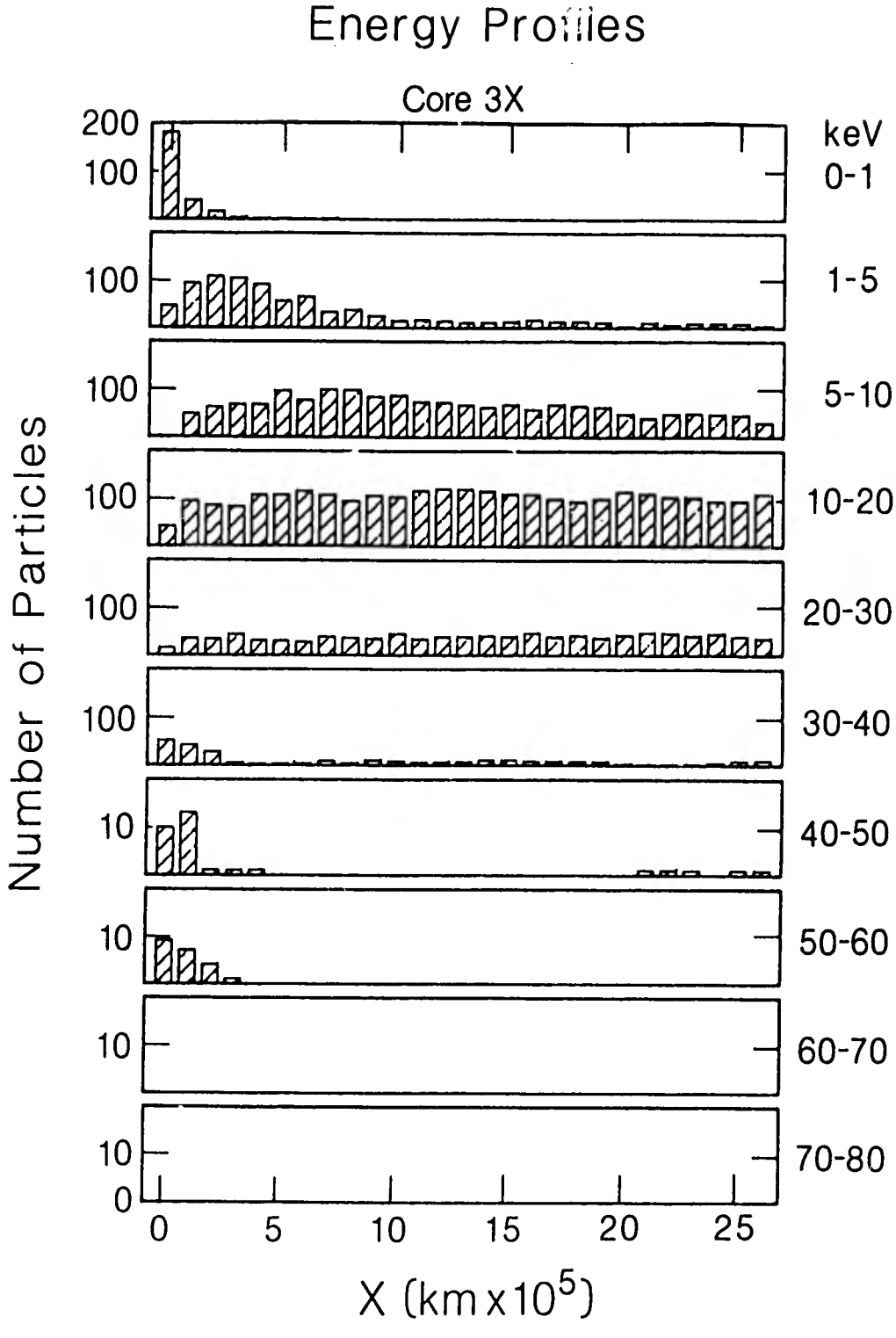

Figure 30. Energy profile for Core 3x showing number of particles with a given energy as a function of x position. Note that close to nucleus (x = 0), most particles have very low energy.

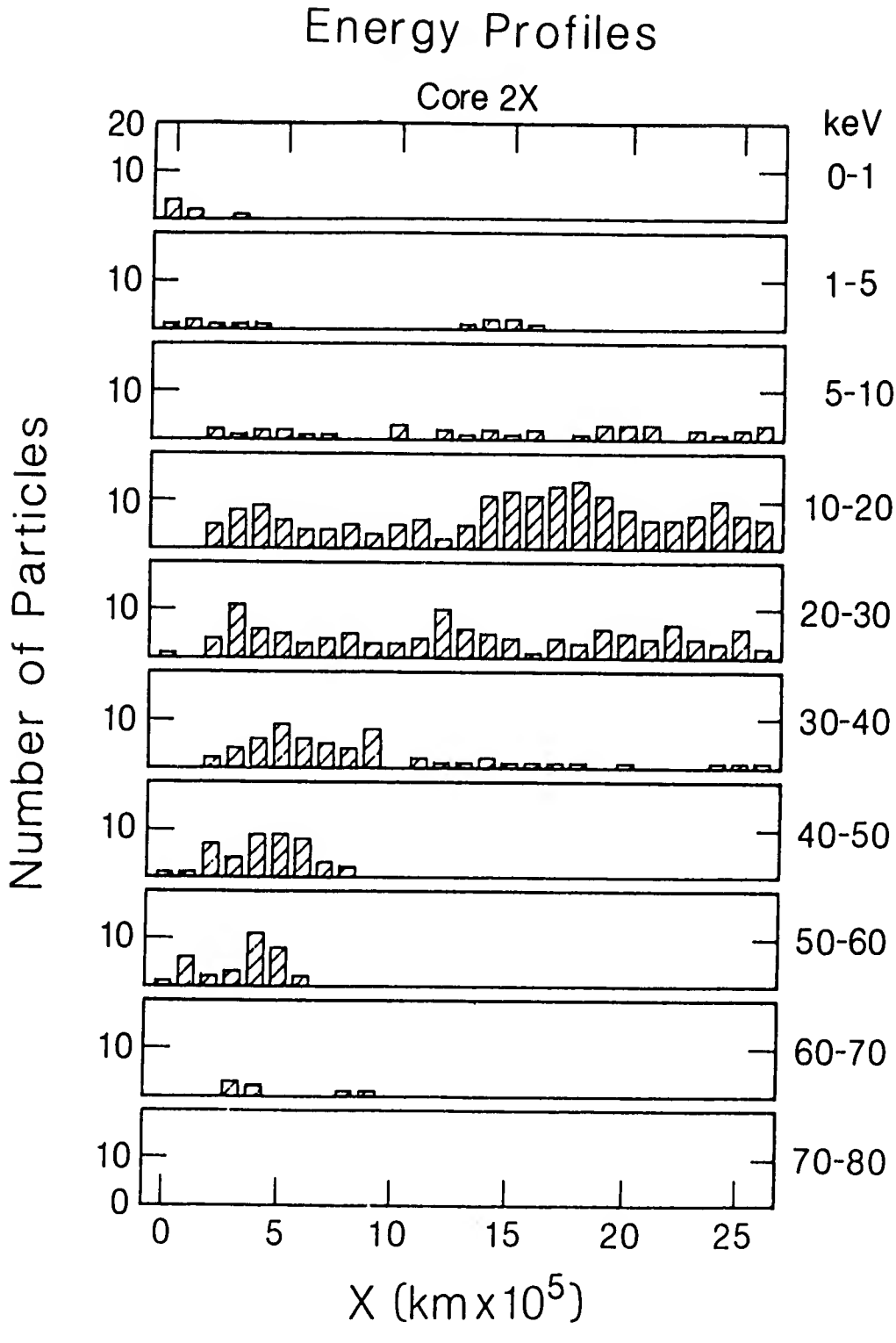

Figure 31. Like Figure 30 for Core 2x. Note particles generally have greater energies in this core, than in the previous core, although the scale is reduced due to the much lower particle number density off the tail axis.

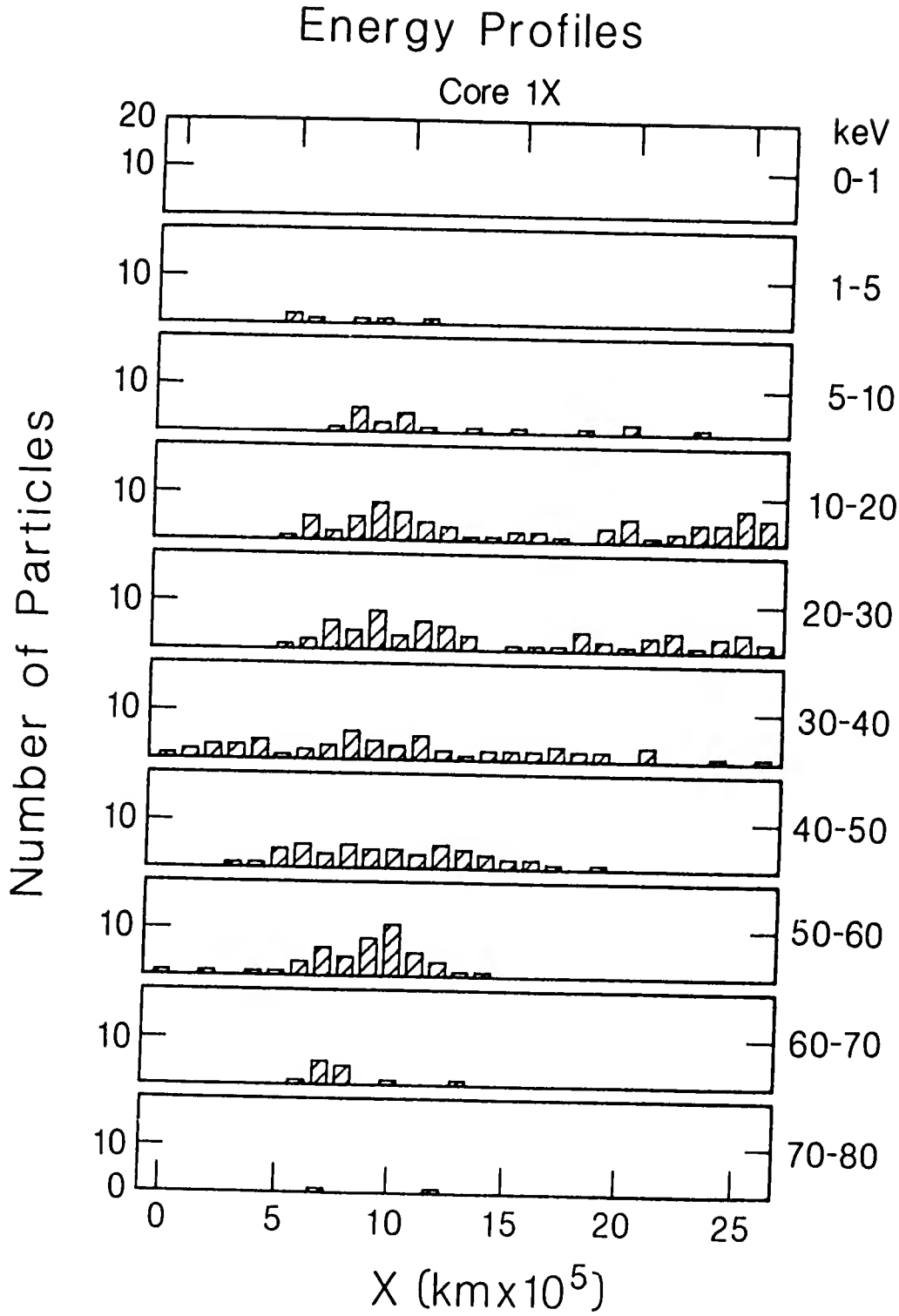

Figure 32. Like Figure 30 for Core 1x. Higher energy particles are appearing farther downstream than in previous core.

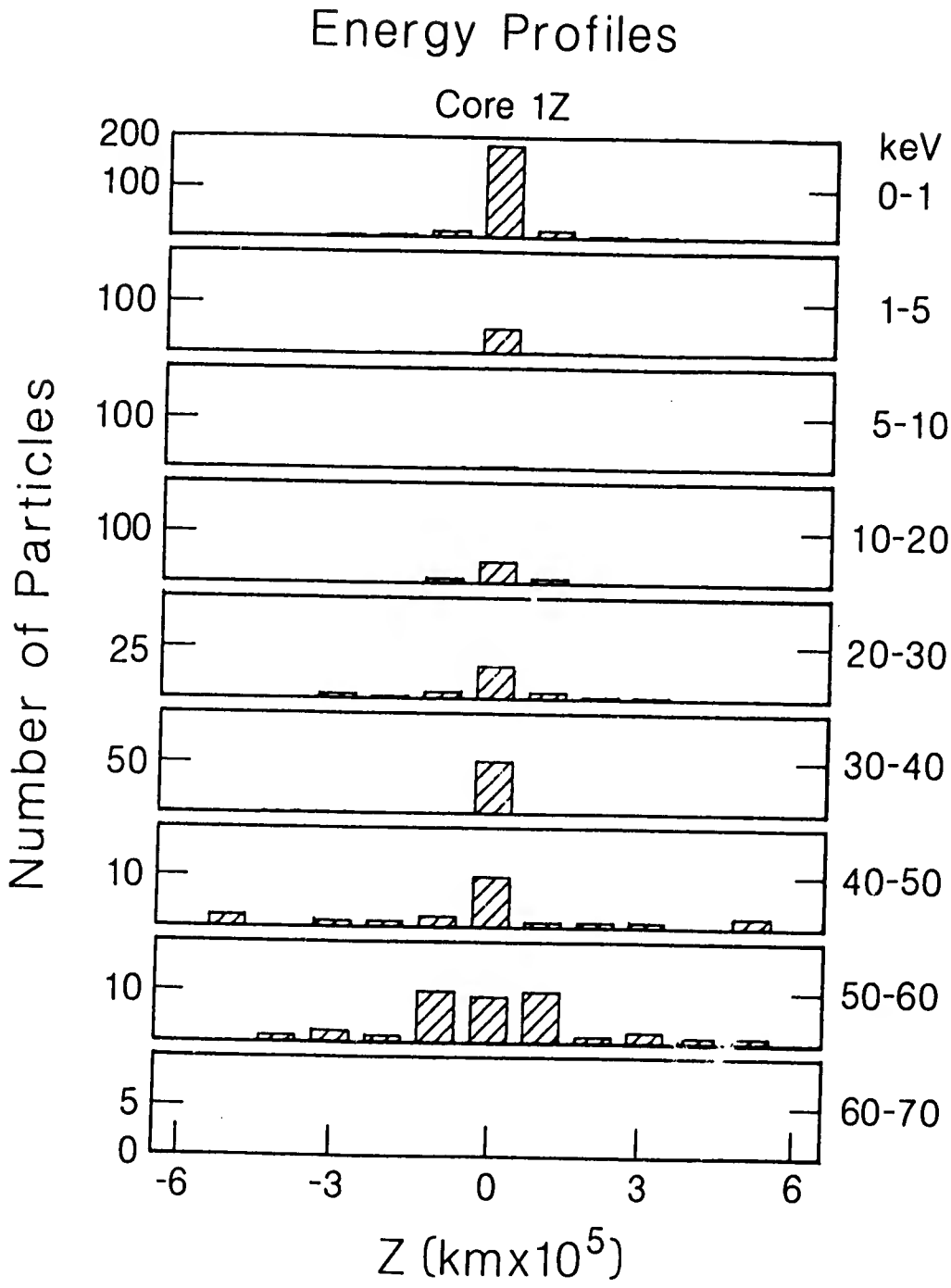

Figure 33. Energy profile for Core 1z showing number of particles with a given energy as a function of z position (z = 0 corresponds to tail axis). Note single-peaked distribution.

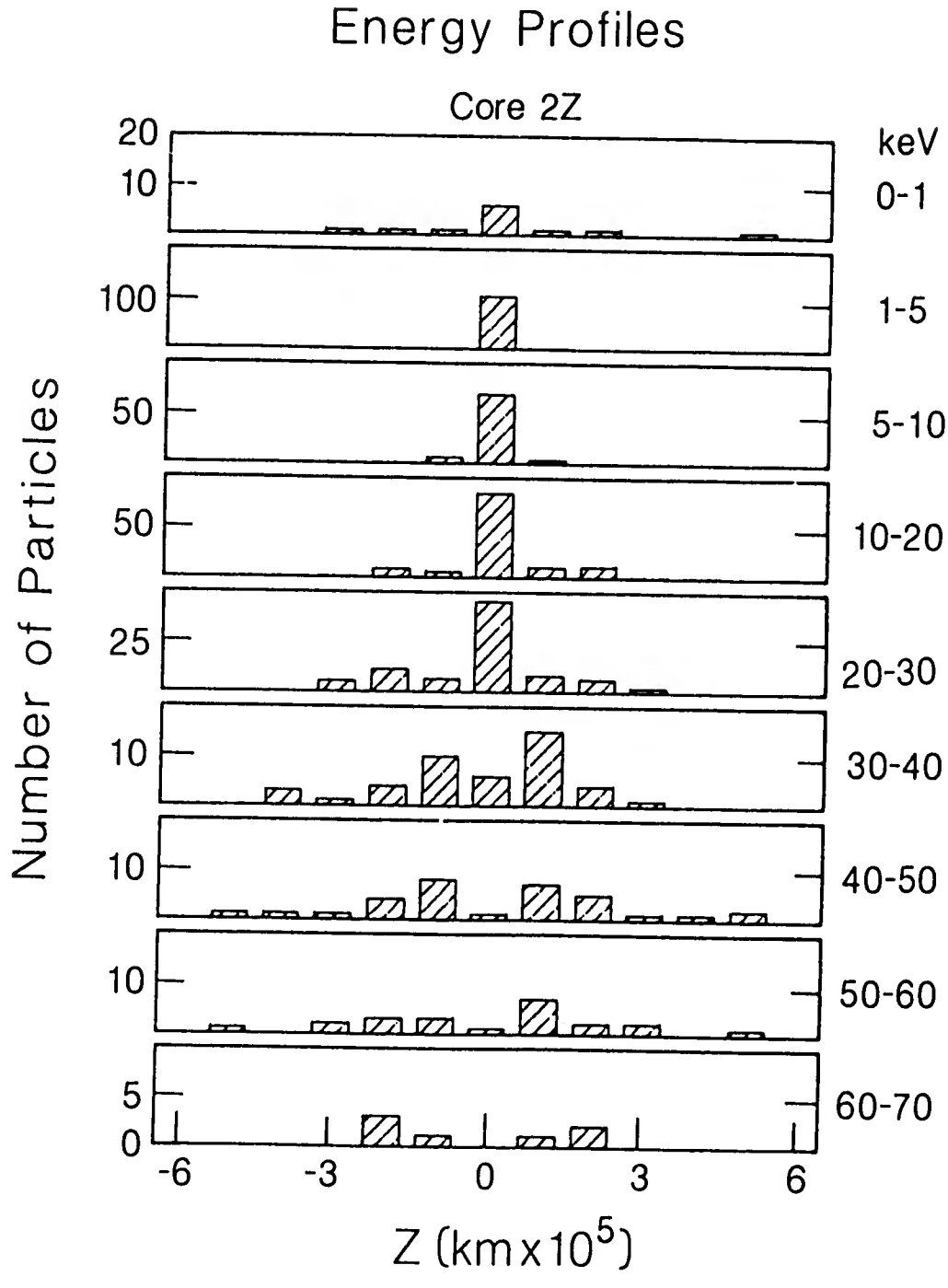

Figure 34. Like Figure 33 for Core 2z. Note transition from single- to double-peaked distribution at the 30-40 keV energy range. This core approximates the ICE trajectory.

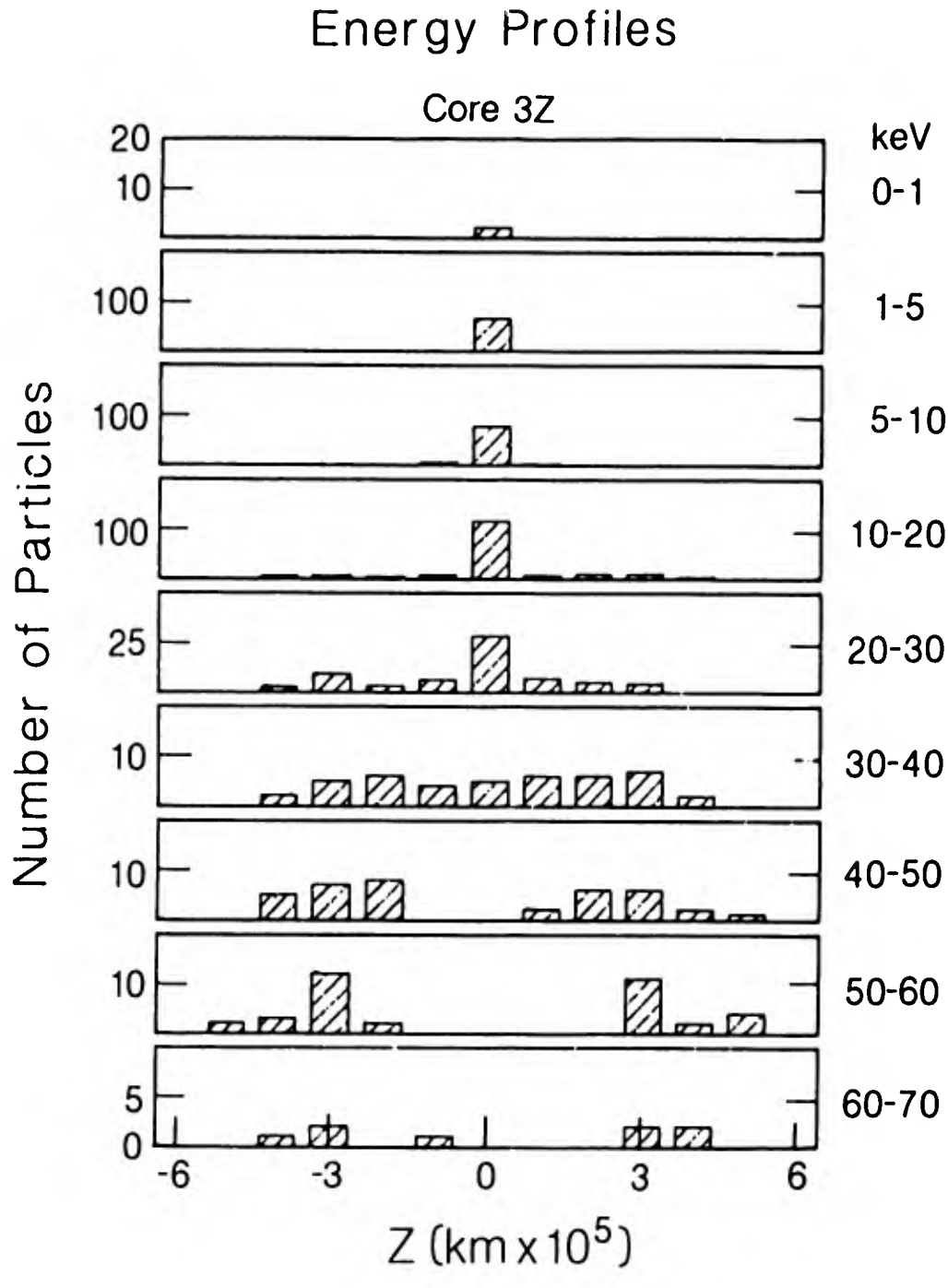

Figure 35. Like Figure 33 for Core 3z. The transition to a double-peaked distribution occurs at a higher energy (40-50 keV) than the previous core and is more pronounced.

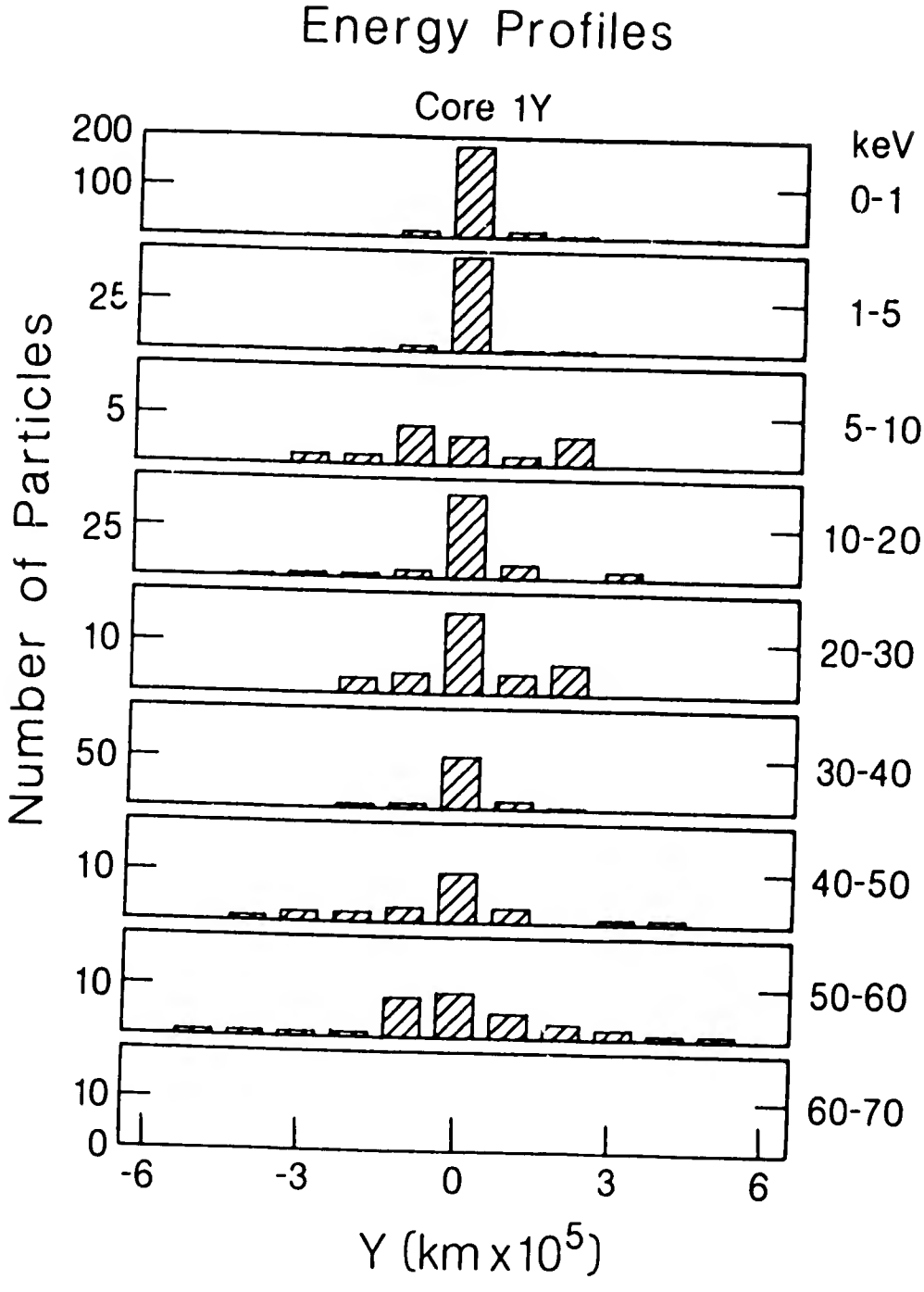

Figure 36. Energy profile for Core 1y showing number of particles with a given energy as a function of y position (x = 0 corresponds to tail axis). Note the single-peaked distribution function.

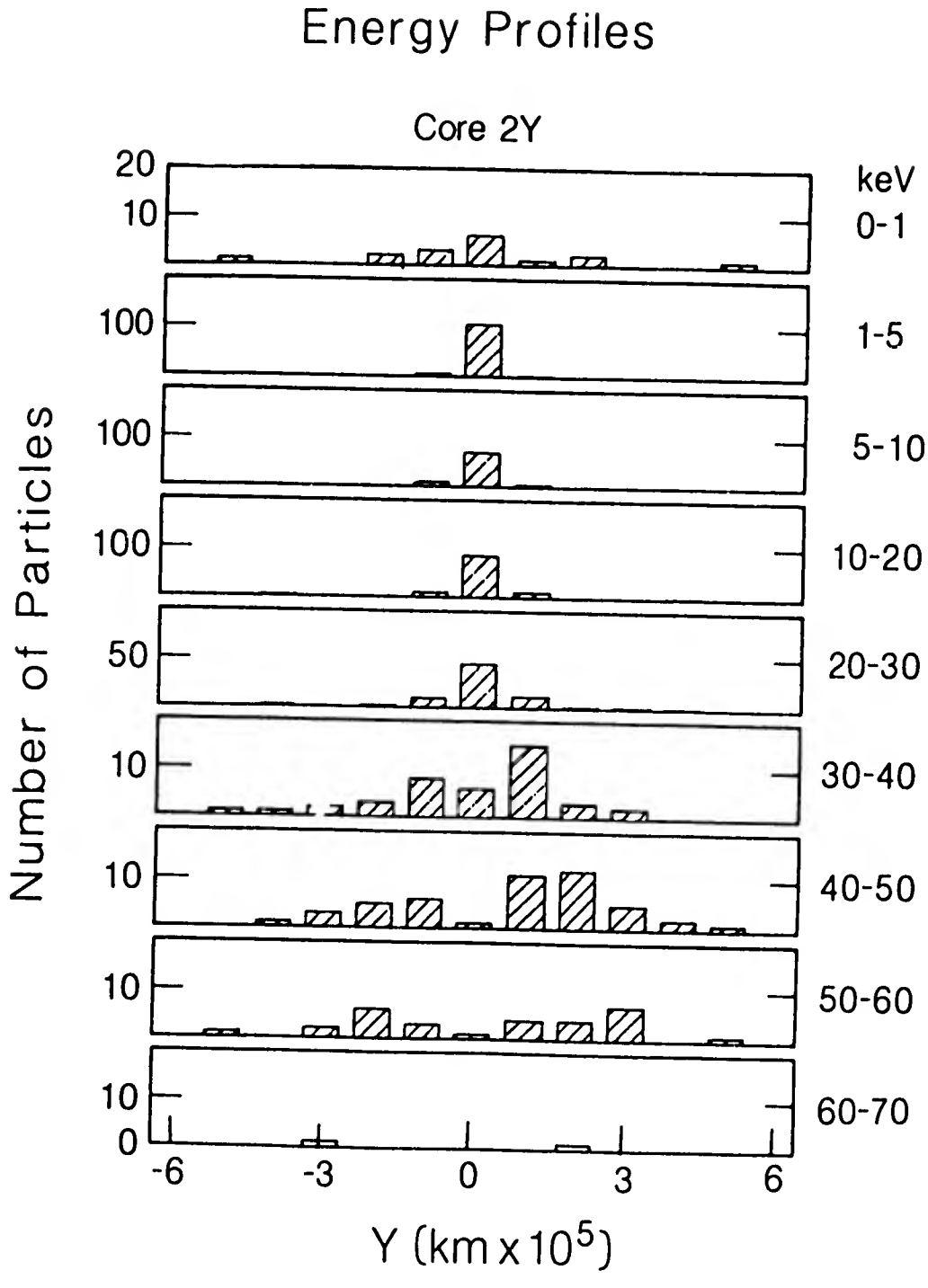

Figure 37. Like Figure 36 for Core 2y. Transition to double-peaked distribution occurs at 30-40 keV.

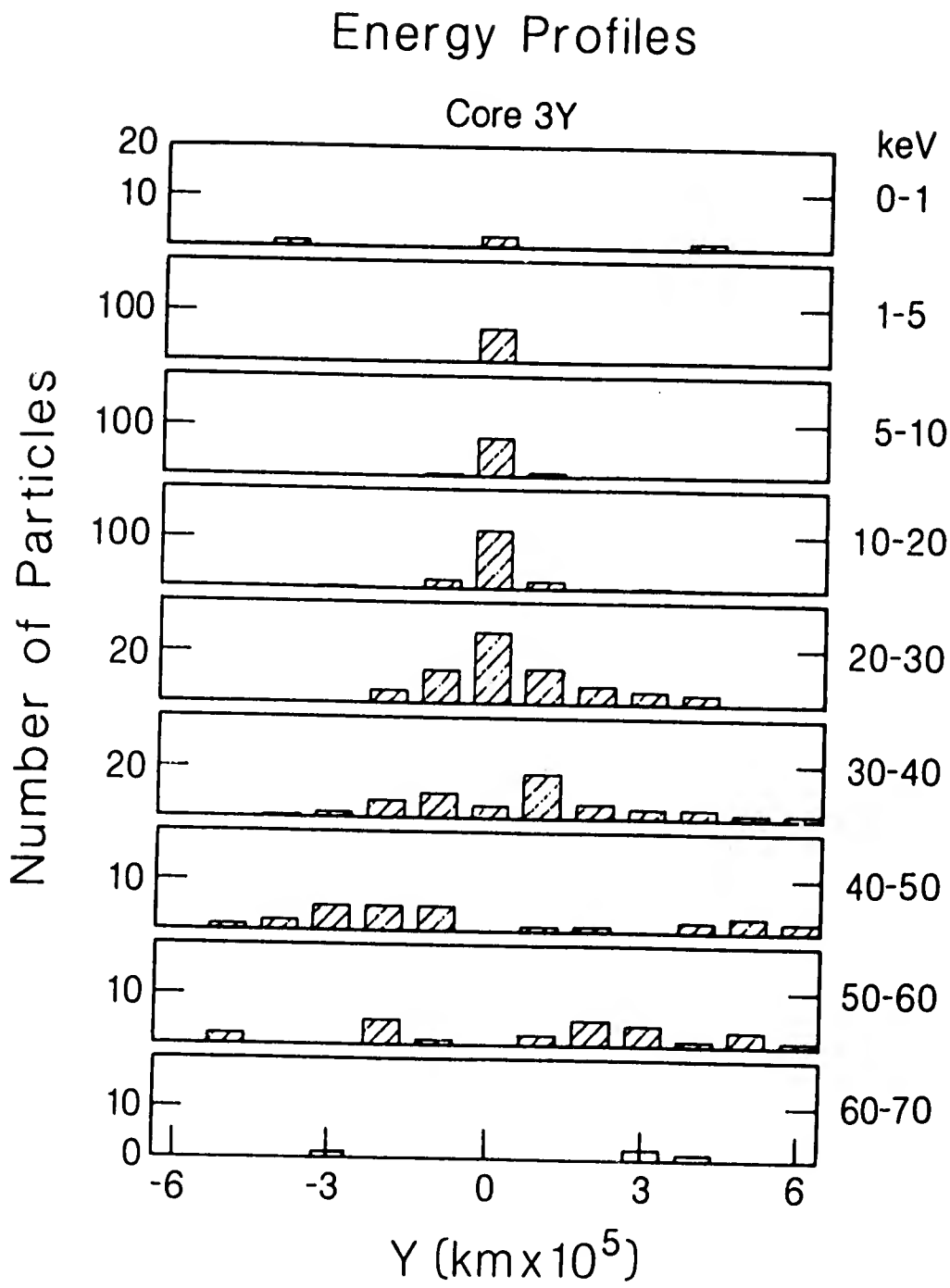

Figure 38. Like Figure 36 for Core 3y. Double-peaked distribution is less pronounced in this plane, orthogonal to the IMF.

The stability of the cometary plasma can be evaluated by examining the phase space distribution of the cometary ions. The examples from selected cubes in Figure 42 illustrate the tendency for ring distributions to occur where the energetic wings are located, while smooth, centrally peaked distributions are found in the region of the colder plasma sheet and wake. Of course, instability theory also requires a knowledge of the distribution function of the background (solar wind) plasmas which is not easily obtained from the single fluid MHD model used here. Nevertheless, results of this type could be used for a crude assessment of the global pattern of the locations where various ion pick-up instabilities arise.

The results displayed above show the predicted behavior of test particles launched in the MHD multidimensional simulation of Comet Giacobini-Zinner. In conjunction with the particle trajectories of the previous chapter, these predictions of the density profile, energy spectra, energy profiles, pitch angle distributions, and phase space distributions provide valuable information on predicted particle behavior at comets. The true test of such a model, however, is how the simulation results compare with actual spacecraft observations. Fortunately, such particle observations were obtained by the ICE spacecraft and will be compared with the above predictions in the next chapter.

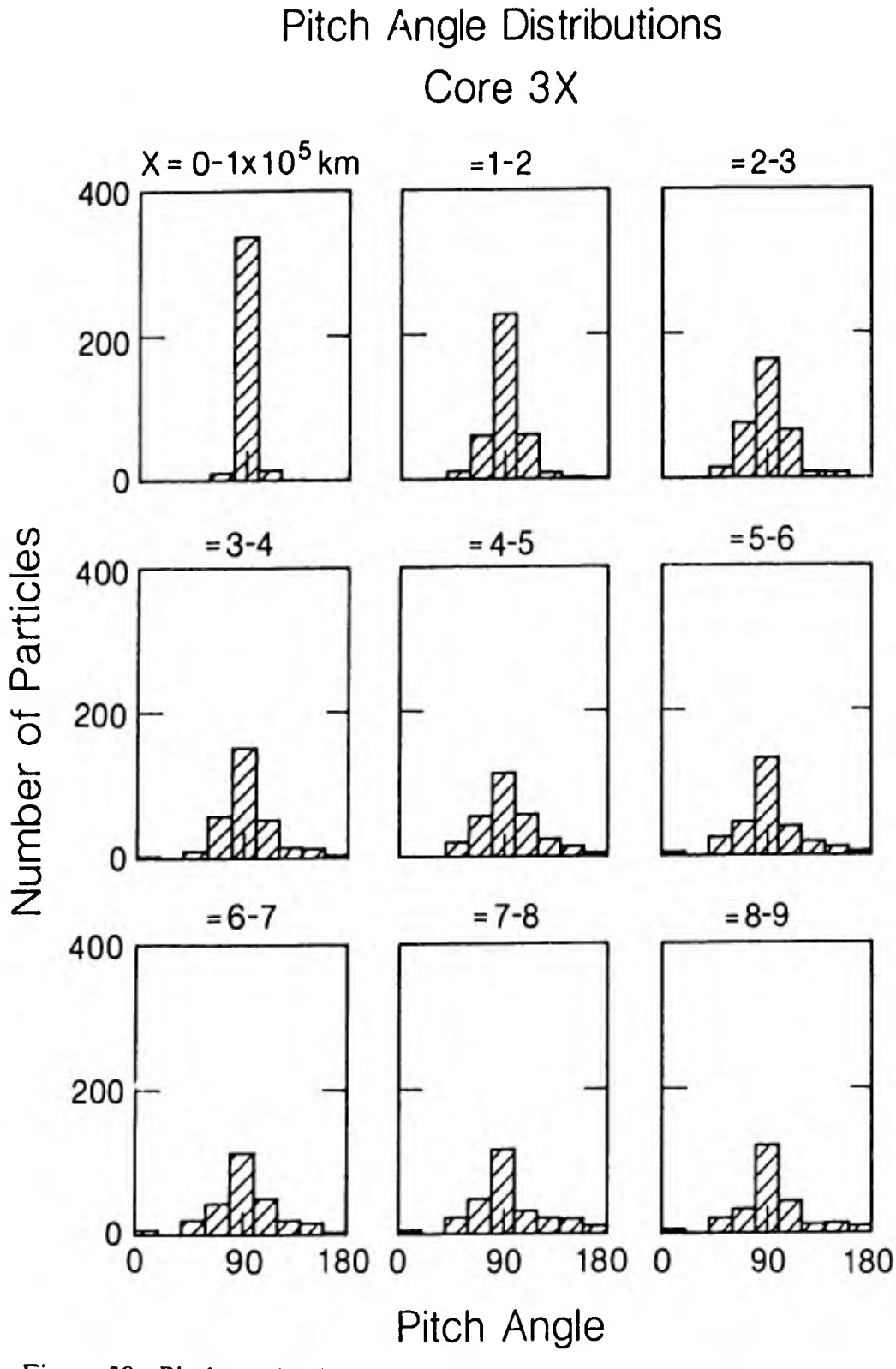

Figure 39. Pitch angle distributions for the first 9 cubes along the tail axis (Core 3x). Note the distributions are centered around 90°, indicating a "pancake" distribution of particles.

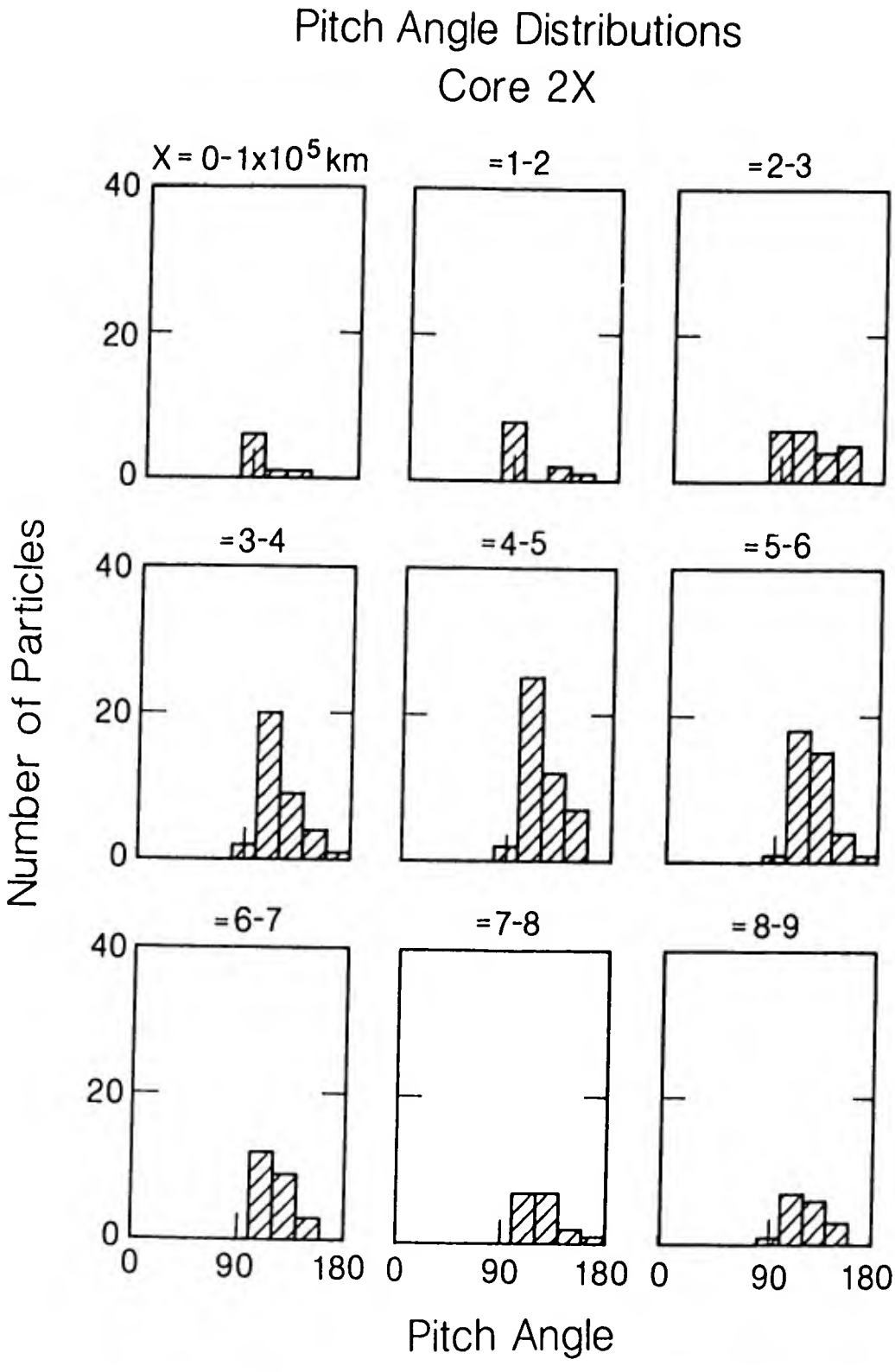

Figure 40. Like Figure 39 for Core 2x. Note the shift of the distribution to a value between 90° and 180°, indicating a "conic" distribution of particles. A similar core on the other side of the tail axis would display pitch angles between 0° and 90°.

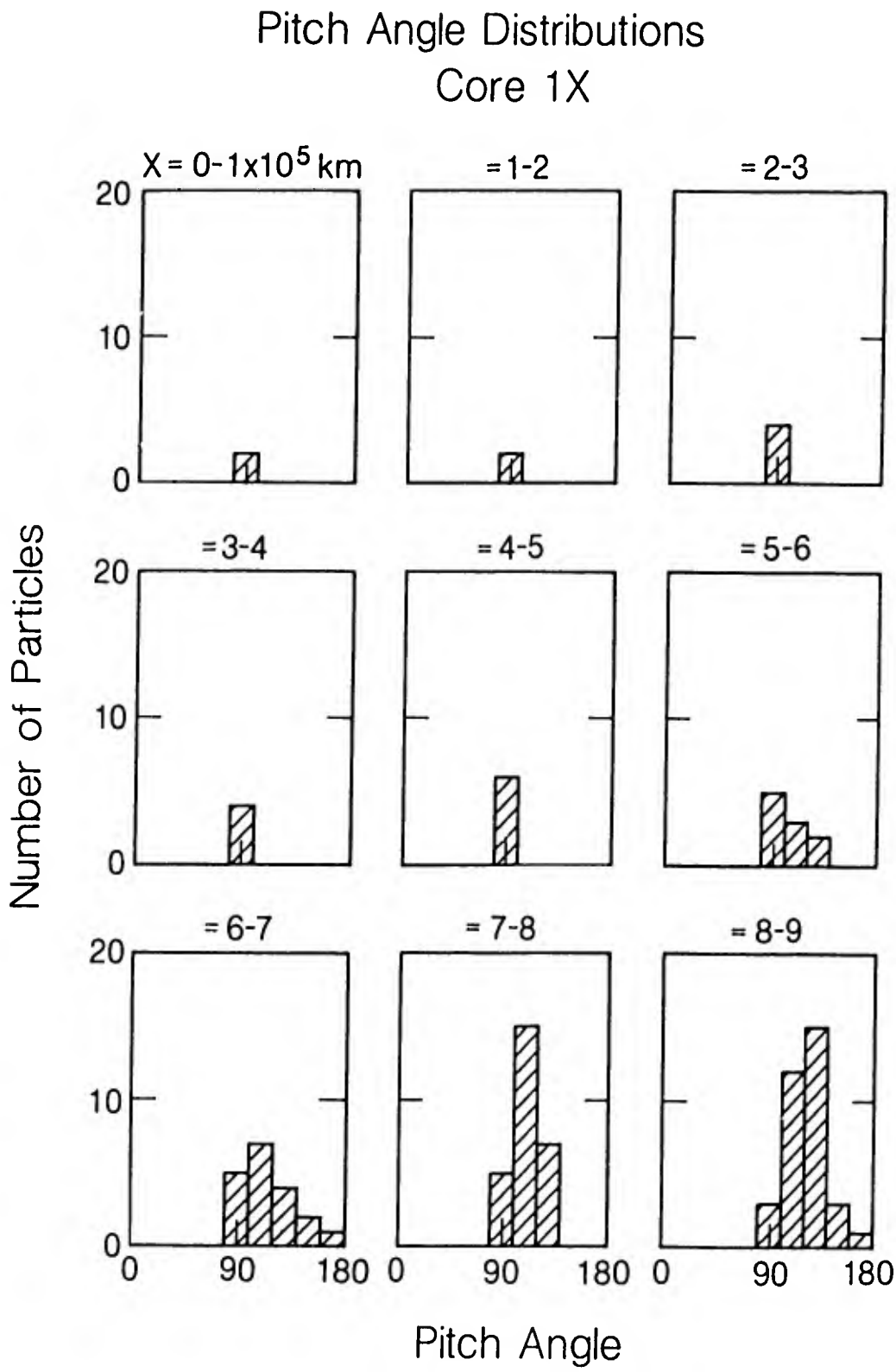

Figure 41. Like Figure 39 for Core 1x. Conic distributions persist.

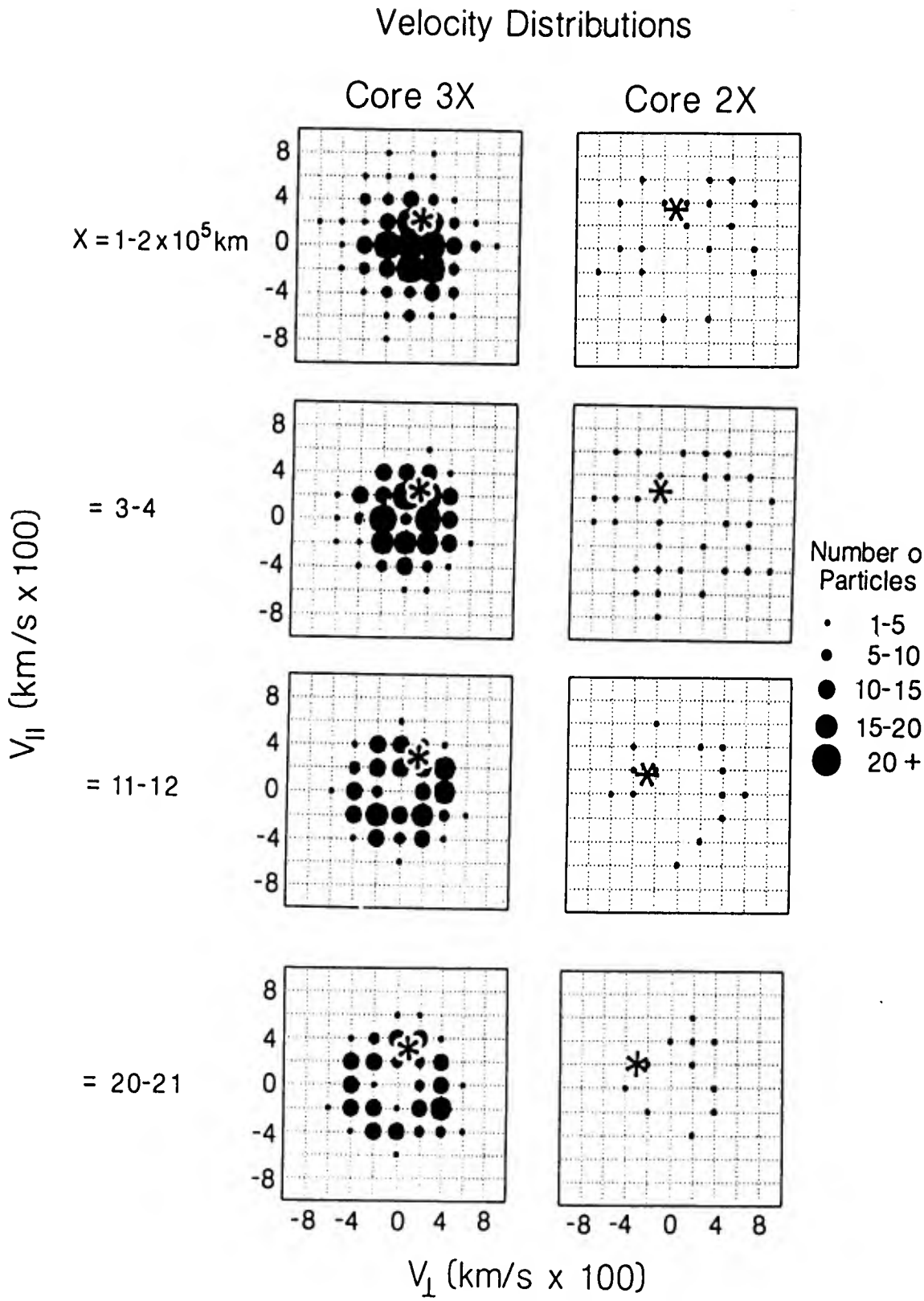

Figure 42. Phase space distributions in velocity space for selected cubes in Core 3x and Core 2x. The asterisk indicates the location of the bulk plasma flow. Note the ring distribution as distance downstream increases.

Chapter VI

COMPARISON OF MODEL RESULTS WITH OBSERVATIONS

The validity of the test particle simulation becomes evident when the results of the simulation are compared directly with the ICE observations. The observations of 35 keV water group ions, as well as higher energy observations in the 65-95 keV range were previously discussed in Chapter II and illustrated in Figure 3. The remarkable feature in both energy ranges was the distinctive "double peak" spatial signature. The results of the simulation can account for the gross features observed at Comet Giacobini-Zinner quite nicely.

By examining the trajectories for either H_2O^+ or CO_2^+ ions, there are clearly two distinct trajectories followed by cold and hot particles, respectively (Figures 15 and 16). The two "wings" in Figures 15 and 16 are composed of "hot" particles separated by a "cold" plasma sheet, as shown in Figure 17. This can be understood as resulting from the particles picked up in the upstream coma (where $\underline{V}_i$ and thus the motional electrical field, $\underline{E} = -\underline{V} \times \underline{B}$ is large), which diverge from or fan out from the tail axis. The ICE spacecraft, on a trajectory most nearly antiparallel to the interplanetary magnetic field (cf. McComas, 1986), would be expected, from the calculations of this model, to encounter energetic particles inbound, colder particles crossing the tail axis plasma sheet, followed by a second maxima in the number of energetic particles encountered during the outbound leg of its passage across the comet's

tail. This is, in fact, exactly what the data show. Quantitative predictions of the observed data may be made from the energy profiles of the simulation, choosing Core 2z (in plane of the IMF, 3×10^5 km antisunward from nucleus) as a close approximation of the ICE trajectory (Figure 34), and considering only the energy range above 30 keV in compliance with ICE's observational limitations. Again, the double-peaked structure is clearly evident. This consistency also holds for the corresponding flythrough in the y direction, Core 2y (in orthogonal plane, 3×10^5 km antisunward of nucleus). The energetic wings of particles, first illustrated in the trajectory plots, later in "slices" through the simulation box, and in Figure 34, are seen to diverge away from the tail axis, producing these double maxima in the data. The energy spectra (Figures 24-29) show that as the distance from the nucleus increases, energetic particles occur farther away from the tail axis (Cube x = 6-7 in z or y).

Data from the pitch angle analysis of the test particles shows the energetic wings developing in the plane of the interplanetary magnetic field. Along the tail axis, Figure 39, the distribution of pitch angles is centered at 90°. Thus almost all a particle's motion is perpendicular to the magnetic field. These cold particles are essentially undergoing $\underline{E} \times \underline{B}$ drift. However, as the distance from the tail axis is increased (Figures 40 and 41), the pitch angle distributions shift to an angle greater than 90°, indicating an acceleration away from the tail axis again consistent with previous results.

A prediction of the stability of the plasma can be made from the phase space distribution plots in Figure 42. In Figure 42, the size of the circles on the $V_{par} - V_{perp}$ grid is directly proportional to the number of particles at a

particular location in $V_{par} - V_{perp}$ space. As increasingly distant cubes are sampled, moving away from the nucleus (moving down column 1, Core 3x), an interesting ring distribution develops. Low velocity particles undergo acceleration, thus the absence of counts at the lowest energies. The bulk plasma velocity, indicated by the *, shows that the distributions are relatively stable throughout the tail axis core, although more stable distributions tend to be located closer to the nucleus. A comparison of a parallel but off-axis core, Core 2x, shows the same general ring distribution, although the statistics are much poorer due to the drastically smaller number of particles in this core.

These results of the trajectory paths, the energy distribution of the particles, profiles of particle density and energy, along with energy spectra, pitch angle distributions, and phase space distributions, all indicate a self-consistent explanation of the observed particle behavior based on single-particle motion in a global MHD simulation. The simulation creates a double-peaked distributions of energetic particles along the z cores that are analogous to what is observed by the ICE spacecraft. This is due to the location of the picked-up ions. Those picked up sunward, or at a great distance from the nucleus where the solar wind velocity is high, are accelerated to higher velocities and energies, forming two wings of energetic particles fanning out primarily in the plane of the interplanetary magnetic field away from the nucleus. Conversely, those particles captured downstream of, or near, the nucleus acquire much less energy due to the correspondingly lower solar wind velocity. This explanation of the observed double-peaked

distribution of pick-up ions is based on the large-scale properties of the plasma and magnetic field only.

Chapter VII

SUMMARY AND CONCLUSIONS

The ICE spacecraft observations of water ions at Comet Giacobini-Zinner are the first *in situ* measurements of such particles. The spacecraft data enable various numerical models of the comet-solar wind interction to be realistically evaluated. Two popular models of this interaction were unable to explain the double-peaked distribution of energetic ions seen in the spacecraft data. This project combined aspects of the two previous models. This study is based on a global MHD simulation of the flow and magnetic field structure surrounding Comet Giacobini-Zinner developed by J.A. Fedder and coworkers. The MHD model is a single fluid model where no distinction is made between solar wind components and cometary components. In this study, the trajectories of 750 test particles contained in the MHD model are analyzed. Test particles are selected based on a realistic density profile of the cometary atmosphere. Thus the test particles effectively simulate the cometary ions. Effects of scattering of the particle trajectories by fluctuations of the plasma and magnetic fields were not evaluated in this study, but those fluctuations are not expected to greatly affect the large-scale features of the particle trajectories. This simulation illustrates the underlying organization of comet ion trajectories by the background magnetic and convection electric fields. The gradient and curvature drifts of the ions due to the magnetic field compressing and bending

around the comet influences the ion trajectories. By analyzing the behavior of individual test particles under the influence of the MHD model magnetic and velocity fields, the observed characteristics of cometary pick-up ions, including the distinctive double-peaked distribution, is produced.

The ion behavior is shown to depend not only on the local conditions of the magnetic and velocity fields, but also on the cumulative effects of upstream field structure. Particles picked up where the solar wind velocity is high become more highly energized than particles picked up by a slow solar wind. High solar wind velocities are found in areas where mass loading has not occurred (i.e., upstream and far from the comet nucleus). When the solar wind picks up cometary ions, mass loading results and the velocity of the solar wind must slow. This slowing of the solar wind occurs close to and downstream of the comet nucleus. The results of this simulation show that the particles picked up by a fast solar wind diverge from the tail axis, forming the hot wings observed by the ICE spacecraft. The comparatively cold particles picked up by a slow, mass-loaded solar wind focus into the tail axis, creating the plasma sheet.

The results of the test particle trajectory analysis reproduce the major features observed by the spacecraft. The density profiles show the bulk of cometary ions concentrated along the tail axis, most near the nucleus. Away from the tail axis, local maxima occur downstream of the nucleus due to the wings of energetic ions. Very cold ions are located near the nucleus, with energies increasing with distance from the nucleus. This increase in energy with distance from the nucleus is due to the decrease in mass loading and

subsequent increase in solar wind velocity. The distinctive double-peak feature in the ICE data appears in the energy profiles orthogonal to the tail axis. In particular, Core 2z most nearly represents the spacecraft trajectory and closely resembles the actual observations. Pitch angle analysis shows the predominance of pancake distributions ($\alpha = 90°$) along the tail axis, while conic distributions are evident away from the tail axis ($90° < \alpha < 180°$). The phase space distributions indicate that a ring distribution develops as the distance down the tail axis increases.

An interesting feature of the simulation is not observed in the spacecraft data. No data of low energy ions (< 30 keV) was obtained by ICE due to an equipment failure. Yet the results of this simulation show that a transition to a single-peaked distribution function occurs for energies of less than 30 keV. This feature appears in both directions orthogonal to the tail axis and is not dependent on distance from the nucleus. The peak is centered on the tail axis. Had ICE been able to detect these lower energy particles, the model predicts that the spacecraft data would show a time series peaked at closest approach, rather than the observed double peaks for higher energy particles.

The results of this project can be applied to the recent observations at Comet Halley. Unlike the Giacobini-Zinner encounter, which traversed the comet downstream of the nucleus, the Halley spacecraft passed upstream (sunward) of the nucleus. This upstream pass may explain in part the much less turbulent plasma and magnetic field observations obtained at Comet Halley (cf. Gloeckler et al., 1986; Johnstone et al., 1986; and Reidler et al., 1986). Perhaps the inbound-outbound asymmetry of the picked-up ion energy

spectra seen by Johnstone et al.'s (1986) experiment around closest approach may be explainable in terms of the dual nature of the picked-up ion population (energetic wings vs. cold plasma sheet). The two peaks can be attributed to the high-energy ions picked up from the upstream coma, and the locally picked-up ions, whose energies are determined by the slow local background plasma flow. From the results of this global MHD simulation of Comet Giacobini-Zinner and the analysis of numerous test particle trajectories, it is concluded that a similar modeling exercise for Comet Halley, using the recently updated plasma and magnetic field structure of that comet, will provide a valuable means of analysis for these most recent ion data. This future study should be more productive due to the full spectrum of ions detected and less turbulence throughout the encounter.

SELECTED REFERENCES

Alfvén, H., On the theory of comet tails, Tellus, 9, 92, 1957.

Amata, E., and V. Formisano, Energization of positive ions in the cometary foreshock region, Planet. Space Sci., 33(11), 1243, 1985.

Baker, D.N., W.C. Feldman, S.P. Gary, D.J. McComas, and J. Middleditch, Plasma fluctuations and large scale mixing near Comet Giacobini-Zinner, Geophys. Res. Lett., 13, 271, 1986.

Biermann, L., Kometenschweife und solare Korpuskular Strahlung, Zs für Astrophysik, 29, 274, 1951.

Boice, D.C., W.F. Huebner, J.J. Keady, H.U. Schmidt, and R. Wegmann, A model of comet P Giacobini-Zinner, Geophys. Res. Lett., 13, 381, 1986.

Cravens, T.E., Ion distribution functions in the vicinity of Comet Giacobini-Zinner, Geophys. Res. Lett., 13(3), 275-278, 1986.

Daly, P.W., T.R. Sanderson, K.P. Wenzel, S.W.H. Cooley, R.H. Hynds, and E.J. Smith, Gyroradius effects on the energetic ions in the tail lobes of Comet P/Giacobini-Zinner, Geophys. Res. Lett., 13, 4, 1986.

Fedder, J.A., J.G. Lyon, and J.L. Giuliani, Jr., Numerical simulations of comets: Predictions for Comet Giacobini-Zinner, Eos Trans. AGU, 67(2), 17, 1986.

Gloeckler, G., M. Scholer, F.M. Ipavich, D. Hovestadt, and B. Klecker, Abundances and spectra of suprathermal H^+, He^{2+} and heavy ions in a fast moving plasma structure (plasmoid) in the distant geotail, Geophys. Res. Lett., 11, 603, 1984.

Gloeckler, G., D. Hovestadt, F.M. Ipavich, M. Scholer, B. Klecker, and A.B. Galvin, Cometary pick-up ions observed near Giacobini-Zinner, Geophys. Res. Lett., 13, 251, 1986.

Gosling, J.T., J.R. Asbridge, S.J. Bame, M.F. Thomsen, and R.D. Zwickl, Large amplitude low frequency plasma fluctuations at Comet Giacobini-Zinner, Geophys. Res. Lett., 13, 267, 1986.

Gringauz, K.I. et al., First *in situ* plasma and neutral gas measurements at Comet Halley, Nature, 321, 282, 1986.

Hovestadt et al., The nuclear and ionic charge distribution particle experiments on the ISEE-1 and ISEE-C spacecraft, IEEE Trans. Geosci. Electron. GE-16, 166, 1978.

Hynds, R.J., S.W.H. Cowley, T.R. Sanderson, J. van Rooijen, and K.P. Wenzel, Observations of energfetic ions from Comet Giacobini-Zinner, Science, 232, 361, 1986.

Ip, W.H., and W.I. Axford, Theories of physical processes in the cometary comae and ion tails, p. 588 in Comets, edited by L.L. Wilkening, University of Arizona Press, 1982.

Ipavich, F.M., A.B. Galvin, G. Gloeckler, D. Hovestadt, B. Klecker, and M. Scholer, Comet Giacobini-Zinner: *In situ* observations of energetic heavy ions, Science, 232, 366, 1986.

Johnstone, A. et al., Ion flow at Comet Halley, Nature, 321, 344, 1986.

Kömle, N.I., and H.I.M. Lichtenegger, Numerical modeling of comet-solar wind interaction, p. 19-36 in Field, Particle and Wave Experiments on Cometary Missions, edited by K. Schwingenschuh and W. Riedler, Graz, Austria, 1986.

McComas, D.J., J.T. Gosling, S.J. Bame, J.A. Slavin, E.J. Smith, and J.L. Steinberg, The Giacobini-Zinner magnetotail: Tail configuration and current sheet, J. Geophys. Res., in press, 1986.

Neubauer, F.M. et al., First results from the Giotto magnetometer experiment at Comet Halley, Nature, 321, 352, 1986.

Reidler, W., K. Schwingenschuh, Ye.G. Yeroshenko, V.A. Styashkin, and C.T. Russell, Magnetic field observations in Comet Halley's coma, Nature, 321, 288, 1986.

Sanderson, T.R., K.P. Wenzel, P. Daly, S.W.H. Cowley, R.J. Hynds, E.J. Smith, S.J. Bame, and R.D. Zwickl, The interaction of heavy ions from Comet P.Giacobini-Zinner with the solar wind, Geophys. Res. Lett., 13, 311, 1986.

Schmidt, H.U., and R.W. Wegmann, Plasma flow and magnetic fields in comets, p. 538 in Comets, edited by L.L. Wilkening, University of Arizona Press, 1982.

Slavin, J.A., E.J. Smith, B.T. Tsurutani, G.L. Siscoe, D.E. Jones, and D.A. Mendis, Giacobini-Zinner magnetotail: ICE magnetic field observations, Geophys. Res. Lett., 13, 283, 1986.

Smith, E.J. et al., International Cometary Explorer encounter with Giacobini-Zinner: Magnetic field observations, Science, 232, 382, 1986.

Terasawa, T., T. Mukai, W. Miyake, M. Kitayama, and K. Hirao, Detection of cometary pick-up ions up to 10^7 km from Comet Halley: Suisei observation, Geophys. Res. Lett., 13, 705, 1986.

Tsurutani, B.T., and E.J. Smith, Strong hydromagnetic turbulence associated with Comet Giacobini-Zinner, Geophys. Res. Lett., 13, 259, 1986.

Walker, R.J., Modeling planetary magnetospheres, Rev. Geophys., 21, 495, 1983.

Wallis, M.K., and A.D. Johnstone, Implanted ions and the draped cometary field, p. 307 in Cometary Exploration I, Proc. International Conf. on Cometary Exploration, edited by T.I. Gombosi, Central Research Inst. for Physics, Hugarian Academy of Sciences, 1982.

Wenzel, K.P., The ICE encounter with Comet Giacobini-Zinner, Proc. International Workshop, 21-23 Oct 1985, Graz, Austria, IWF-Preprint 8601.

Whipple, F.L., A comet model. I. The acceleration of Comet Encke, Astrophys. J., 111, 375, 1950.

Winske, D., C.S. Wu, Y.Y. Li, Z.Z. Mou, and S.Y. Guo, Coupling of newborn ions to the solar wind by electromagnetic instabilities and their interaction with the bow shock, J. Geophys. Res., 90, 2713, 1985.

Wu, C.S., D. Winske, and J.D. Gaffey, Jr., Rapid pick-up of cometary ions due to strong magnetic turbulence, Geophys. Res. Lett., 13, 865, 1986.

Yeomans, D.K., and J.C. Brandt, The Comet Giacobini-Zinner Handbook, Report JPL 400-254, NASA, Washington, D.C., 1985.